

Phenomenology in minimal cascade seesaw for neutrino mass

Ran Ding ^{a,*}, Zhi-Long Han ^{a,†}, Yi Liao ^{a,c,‡}, Hong-Jun Liu ^{a,§} and Ji-Yuan Liu ^{b,¶}

^a *School of Physics, Nankai University, Tianjin 300071, China*

^b *College of Science, Tianjin University of Technology, Tianjin 300384, China*

^c *Kavli Institute for Theoretical Physics China, CAS, Beijing 100190, China*

Abstract

We make a comprehensive analysis on the phenomenology in the minimal version of cascade seesaw for tiny neutrino mass. The seesaw induces at tree level a neutrino mass operator at dimension nine, by introducing a quadruple scalar Φ of hypercharge unity and a quintuple fermion Σ of hypercharge zero. We work in a framework that handles the complicated Yukawa couplings in a nice way without losing generality. All mixing matrices are essentially expressed in terms of the vacuum expectation value of the quadruple scalar v_Φ , a free complex parameter t , and known neutrino parameters. We show that the low-energy lepton flavor violating transitions of the charged leptons set strong constraints on the free parameters. The constraints have a significant impact on collider physics, and are incorporated in our signal analysis at the LHC. We investigate the signatures of new particles by surveying potentially important channels. We find that the $4j2\ell^\pm$ signal is most important for the detection of the scalars and the $2\ell^\pm 2\ell^\mp 2j$, $3\ell^\pm \ell^\mp 2j$ and $3\ell^\pm 2\ell^\mp + \cancel{E}_T$ signals are quite promising for the fermions.

*Electronic address: dingran@mail.nankai.edu.cn

†Electronic address: hanzhilong@mail.nankai.edu.cn

‡Electronic address: liaoy@nankai.edu.cn

§Electronic address: liuhj@mail.nankai.edu.cn

¶Electronic address: liujy@tjut.edu.cn

I. INTRODUCTION

The origin of tiny yet nonvanishing neutrino mass has remained mysterious since its discovery in oscillation experiments. Although such a tiny mass can be incorporated by a trivial extension of the standard model (SM) with right-handed neutrinos, it has to appeal to unnaturally small Yukawa couplings. In this circumstance, it is more useful to regard SM as an effective field theory in which the neutrino mass appears as a low energy remnant of some high scale physics. Such low energy effects can be systematically organized by higher dimensional operators in terms of the SM fields. Indeed, it has been known for long that such an operator, that is relevant to neutrino mass, first appears at dimension five and has the unique form, $\mathcal{O}_5 = \left(\overline{F_L^C} \varepsilon \phi\right) \left(\phi^T \varepsilon F_L\right)$, the so-called Weinberg operator [1]. Here F_L and ϕ are respectively the SM left-handed lepton doublet and Higgs doublet, and ε is the antisymmetric matrix in the weak isospin space. The operator is suppressed by an effective coupling λ/Λ , where Λ is a heavy mass scale and λ a product of fundamental couplings of some new physics.

What high scale new physics would be responsible for the operator \mathcal{O}_5 , and is it accessible in current experiments? A nice analysis shows [2] that, if the operator is a tree level effect of some high-scale fundamental physics, there are three and only three ways to realize it. It is amusing that they correspond exactly to the three types of conventional seesaws that were suggested previously from different points of view [3–5]. While completely equivalent as far as the neutrino mass at low energies is concerned, these seesaws are indeed vastly different at high energies. The issue becomes whether they are discernable in the current or near-future experiments, in particular at the Large Hadron Collider (LHC).

The LHC physics of the three seesaws has been explored in this spirit. The type I seesaw introduces singlet neutrinos whose impact on SM physics enters mainly through their mixing with the SM neutrinos (see, e.g., Ref. [6–10]). This is generically very hard to detect since an appreciable mixing clashes apparently with the desire of tiny neutrino mass and not too heavy new particles. The seesaw has thus been studied in an effective sense, namely by decoupling the correlation between the heavy mass and mixing parameters that would appear in a genuine type I seesaw. In type II seesaw one assumes a scalar triplet carrying the same hypercharge as the SM Higgs. The tininess of neutrino mass is then shared by the vacuum expectation value (VEV) of the triplet and its Yukawa coupling to leptons. The phenomenology of type II seesaw is rich, and has been extensively investigated in the literature [11–14]. The type III seesaw attributes the

tiny neutrino mass to the mixing with heavy triplet fermions of zero hypercharge. This seesaw is potentially rich in phenomenology but more involved than type II, and has been studied in [15–17]. A comparative study has been made on all three seesaws in Ref. [18]. Both CMS and ATLAS groups at LHC have set constraints on those seesaws based on various simplifying assumptions [19–24], which will be briefly discussed in section IV. Due to the residual tension in the conventional seesaws between heavy mass and small couplings, there are attempts that combine them in one way or another, or include additional structures; see for example, Ref. [25] for the inverse seesaw as an alternative realization of the type I seesaw and Refs. [26, 27] for its variants. For a partial list of more references, see, [18, 28–35].

Because of the tension mentioned above, it is natural to try to go beyond the conventional seesaws. One approach is to diminish the effect of the operator \mathcal{O}_5 by associating it with additional factors of couplings and loop factors. This is achieved usually by employing heavy particles that carry new exact or softly broken discrete symmetries, so that the operator can only be induced at the loop level [36–38]. This helps to alleviate the tendency to accommodate tiny neutrino mass by inaccessible heavy particles and minute couplings to SM particles. An interesting example in this context is the so-called color-octet model [39] in which neutrinos gain mass by interacting with new colored particles that could be detectable [40] at LHC.

A second approach to relax the tension is to raise the dimension of leading operators that are responsible for the neutrino mass, so that they are naturally suppressed by more factors of a high scale. We recall that regarding SM as an effective field theory the neutrino mass operators are unique at each dimension and have the simple form, $\mathcal{O}_{5+2n} = \mathcal{O}_5(\phi^\dagger\phi)^n$, where n is a positive integer [41]. For this to work at the tree level, one has to appeal to heavy particles that constitute a higher dimensional irreducible representation of the SM gauge group [42–44]. It has been shown in Ref. [44] that, by choosing the representations judiciously, a higher-dimensional operator can be induced in a systematical and economical manner: the seesaw operates step by step through a cascading process, with each step offering certain amount of suppression. Such models typically contain multiply charged particles that have characteristic decay modes into like-sign multiple leptons or W^\pm bosons, which could be utilized to remove the SM backgrounds. The purpose of this work is to explore the feasibility of detecting new particles in the minimal version of the cascade seesaw models.

In the next section we outline the basic idea of the cascade seesaw and describe in detail its minimal version whose phenomenology will be investigated in the remainder of the paper. In

section III, we work out the lepton flavor violating (LFV) transitions at low energies that are induced in the model. They turn out to set stringent constraints on the model parameters, and make our analysis of LHC physics more realistic. The decays of new particles, their production and detection channels at LHC are studied in section IV. A brief summary of our main results is recapitulated in the last section. Some details of the model, decays, and loop functions are reserved to several appendices.

II. THE MODEL

There are too many possible ways to introduce new fields in order to induce a higher dimensional neutrino mass operator at the tree level. It was proposed in Ref. [44] to use as our criteria the following points. First, for a given set of fields, we assume that the lowest dimension operator \mathcal{O}_{5+2n} dominates the neutrino mass; namely, we do not consider accidental cancellations in the couplings associated with the mass operators. Second, for a given mass operator, we employ as few new fields as possible to realize it. And finally, we do not impose any symmetry other than the SM gauge symmetries. After a careful analysis, the consequences turn out to be very simple [44]. Both new scalars Φ and fermions Σ are necessary to go beyond the three conventional seesaws. And the possibilities are classified according to whether the SM Higgs ϕ couples to the new fermions Σ or not. If it does, the option is unique – we need a fermion of weak isospin and hypercharge $(I, Y) = (1, 2)$ and a scalar of $(I, Y) = (3/2, 3)$. This is the model composed earlier in Ref. [43] which yields the operator \mathcal{O}_7 for the neutrino mass. If ϕ does not couple to Σ , the result is a class of models [44]. We need one fermion Σ with $(I, Y) = (n+1, 0)$ with integer $n \geq 1$ and a sequence of scalars $\Phi^{(m+1/2)}$ of $(I, Y) = (m+1/2, 1)$ with $m = 1, 2, \dots, n$. The SM gauge symmetries dictate that only the scalar of the highest isospin, $\Phi^{(n+1/2)}$, can have a Yukawa coupling to the fermions Σ and F_L , and that only the scalar of the lowest isospin, $\Phi^{(3/2)}$, can develop a naturally small VEV from interactions with the SM Higgs ϕ . The VEV is then transmitted by a cascading procedure from $\Phi^{(3/2)}$ up to $\Phi^{(n+1/2)}$ through scalar interactions, at each step earning an additional suppression from heavy scalar masses. The end result is a neutrino mass operator \mathcal{O}_{5+4n} that is multiplied by the square of the VEV and Yukawa coupling of $\Phi^{(n+1/2)}$.

In this work, we focus on the minimal version of the cascade seesaw; i.e., we introduce one scalar Φ with $(I, Y) = (3/2, 1)$ and one fermion Σ with $(I, Y) = (2, 0)$, whose members are

$$\Phi = (\Phi_{+2}, \Phi_{+1}, \Phi_0, \Phi_{-1}), \quad \Sigma = (\Sigma_{+2}, \Sigma_{+1}, \Sigma_0, \Sigma_{-1}, \Sigma_{-2}), \quad (1)$$

where the subscripts refer to the electric charge. The SM Higgs doublet and lepton fields are,

$$\phi = (\phi_+, \phi_0), F_L = (n_L, f_L), f_R, \quad (2)$$

where the subscripts L, R denote the chirality. We describe some details of the model in the remainder of this section.

A. Scalars

The complete scalar potential is

$$\begin{aligned} V = & -\mu_\phi^2 \phi^\dagger \phi + \lambda_\phi (\phi^\dagger \phi)^2 + \mu_\Phi^2 \Phi^\dagger \Phi \\ & -\lambda_1 (\Phi \tilde{\Phi})_0 (\phi \tilde{\phi})_0 - \lambda_2 ((\Phi \tilde{\Phi})_1 (\phi \tilde{\phi})_1)_0 + \lambda_3 ((\Phi \Phi)_1 (\tilde{\Phi} \tilde{\Phi})_1)_0 + \lambda_4 ((\Phi \Phi)_3 (\tilde{\Phi} \tilde{\Phi})_3)_0 \\ & - [\kappa_1 (\Phi \tilde{\phi} \phi \tilde{\phi})_0 + \text{h.c.}] - [\kappa_2 ((\Phi \Phi)_1 (\tilde{\phi} \tilde{\phi})_1)_0 + \text{h.c.}] - [\kappa_3 ((\Phi \Phi)_1 (\tilde{\Phi} \tilde{\phi})_1)_0 + \text{h.c.}], \quad (3) \end{aligned}$$

where $\tilde{\Phi} = (\Phi_{-1}^*, -\Phi_0^*, \Phi_{+1}^*, -\Phi_{+2}^*)$ and $\tilde{\phi} = (\phi_0^*, -\phi_+^*)$ transfer under weak isospin precisely as Φ and ϕ respectively. The subscript to a pair of parentheses refers to the isospin of the normalized product inside which is obtained by Clebsch-Gordan coefficients. The couplings $\kappa_{1,2,3}$ are generally complex and the other parameters are real. Together with the Yukawa couplings to be discussed in the next subsection, the $\kappa_{1,3}$ terms violate the lepton number by one unit and the κ_2 term by two units, thus it looks plausible to assume $\kappa_2 \sim \kappa_{1,3}^2$. For simplicity, we will assume when diagonalizing the scalar masses that $\kappa_1 \approx \kappa_3 \approx \kappa$ and $\kappa_2 \approx \kappa^2$ with κ being real. We assume $\mu_\phi^2 > 0$ and $\mu_\Phi^2 > 0$ so that Φ can only develop a naturally small VEV out of that of ϕ . For small κ 's and perturbative λ 's, they are found to be

$$v_\phi \approx \sqrt{\frac{\mu_\phi^2}{2\lambda_\phi}}, \quad v_\Phi \approx \frac{\kappa_1 v_\phi}{2\sqrt{3}r_\Phi}, \quad (4)$$

where $r_\Phi = \mu_\Phi^2/v_\phi^2 + \lambda_1/(2\sqrt{2}) + \lambda_2/(2\sqrt{30})$. Inspection of the second derivatives of V confirms that this is indeed the correct vacuum.

The neutral and singly-charged members of ϕ and Φ mix respectively due to the small κ terms. Denoting $X_0 = (\text{Re}X_0 + i\text{Im}X_0)/\sqrt{2}$ for $X = \Phi, \phi$, the mass matrices for $(\text{Re}\Phi_0, \text{Re}\phi_0)$ and $(\text{Im}\Phi_0, \text{Im}\phi_0)$ are diagonalized approximately by the mixing angles respectively,

$$\theta_R \approx \frac{\sqrt{2}\lambda_1 + 2\lambda_2/\sqrt{30} - 6r_\Phi}{4\sqrt{3}r_\Phi(r_\Phi - 4\lambda_\phi)}\kappa, \quad \theta_I \approx -\frac{1}{2\sqrt{3}r_\Phi}\kappa. \quad (5)$$

The physical states are the CP-even H_0 , h and the CP-odd A_0 respectively. Their masses are only modified by $O(\kappa^2)$ terms, which are safely ignored. The other state from the imaginary fields is the would-be Goldstone field $G^0 = \text{Im}\phi_0 + \kappa/(2\sqrt{3}r_\Phi)\text{Im}\Phi_0$. For the singly charged fields, $(\Phi_{+1}, \Phi_{-1}^*, \phi_+)$, noting that there is no mixing between Φ_{+1} and Φ_{-1}^* , the $\Phi_{+1} - \phi_+$ and $\Phi_{-1}^* - \phi_+$ mixing is diagonalized by the angle ω and ϖ respectively,

$$\omega \approx -\frac{1}{\sqrt{3}r_\Phi}\kappa, \quad \varpi \approx \frac{1}{2r_\Phi}\kappa. \quad (6)$$

Two of the eigenstates have approximately a mass of Φ_{+1} and Φ_{-1}^* , and the third one is the would-be Goldstone $G^+ = \phi_+ + \kappa/(\sqrt{3}r_\Phi)\Phi_{+1} - \kappa/(2r_\Phi)\Phi_{-1}^*$.

The gauge covariant derivative is standard,

$$D = \partial - i\frac{g_2}{\sqrt{2}}(I_+W^+ + I_-W^-) - i\frac{g_2}{c_W}(I_3 - Qs_W^2)Z - ieQA, \quad (7)$$

with the usual notations, $s_W = \sin\theta_W$, $c_W = \cos\theta_W$. For a field of weak isospin 3/2 and unity hypercharge like Φ , one has

$$I_+^\dagger = I_- = \begin{pmatrix} 0 & & & \\ \sqrt{3} & 0 & & \\ & 2 & 0 & \\ & & \sqrt{3} & 0 \end{pmatrix}, \quad I_3 = \text{diag}\left(\frac{3}{2}, \frac{1}{2}, \frac{-1}{2}, \frac{-3}{2}\right), \quad Q = \text{diag}(2, 1, 0, -1). \quad (8)$$

The masses of the W and Z bosons are modified by $O(\kappa^2)$ terms

$$m_W \approx \frac{g_2 v_\phi}{\sqrt{2}} \left(1 + \frac{7}{24r_\Phi^2}\kappa^2\right), \quad m_Z \approx \frac{g_2 v_\phi}{\sqrt{2}} \left(1 + \frac{1}{24r_\Phi^2}\kappa^2\right), \quad (9)$$

resulting in a negligible deviation from unity in the ρ parameter, $\rho - 1 \approx \kappa^2/(4r_\Phi^2)$. The gauge couplings of Φ are recorded in Appendix A.

B. Fermions

We employ here a vector-like fermion Σ with both left-handed and right-handed chiralities. Denoting its Dirac-barred field by $\bar{\Sigma}$ that transforms under isospin as Σ itself and has the components in the order of descendent I_3 ,

$$\bar{\Sigma}_{-2}, \quad -\bar{\Sigma}_{-1}, \quad \bar{\Sigma}_0, \quad -\bar{\Sigma}_{+1}, \quad \bar{\Sigma}_{+2},$$

the Yukawa couplings involving Φ are

$$-\mathcal{L}_{\Phi}^{\text{Yuk}} = 2\sqrt{5} \left[x_i (\overline{F}_{Li}^C \Phi \Sigma)_0 + z_i (\tilde{\Sigma} \Phi F_{Li})_0 + \text{h.c.} \right], \quad (10)$$

where the sum over generation $i = 1, 2, 3$ is understood. Redefining the fermion fields,

$$\begin{aligned} \Sigma_{1L}^0 &= \frac{1}{\sqrt{2}} (\Sigma_{0L} + \Sigma_{0R}^C), \quad \Sigma_{2L}^0 = \frac{i}{\sqrt{2}} (\Sigma_{0L} - \Sigma_{0R}^C), \\ \Sigma_1^- &= \frac{1}{\sqrt{2}} (\Sigma_{-1} - \Sigma_{+1}^C), \quad \Sigma_2^- = \frac{i}{\sqrt{2}} (\Sigma_{-1} + \Sigma_{+1}^C), \\ \Sigma_1^{--} &= \frac{1}{\sqrt{2}} (\Sigma_{-2} + \Sigma_{+2}^C), \quad \Sigma_2^{--} = \frac{i}{\sqrt{2}} (\Sigma_{-2} - \Sigma_{+2}^C), \end{aligned} \quad (11)$$

the Yukawa couplings can be rewritten as

$$-\mathcal{L}_{\Phi}^{\text{Yuk}} = \sum_{m=-2}^{+2} Y_{ix}^m \left[\sqrt{2+m} \Phi_m \overline{\Sigma}_x^m P_L n_i + \sqrt{2-m} \Phi_{m+1} \overline{\Sigma}_x^m P_L f_i \right] + \text{h.c.} . \quad (12)$$

where the sum over $x = 1, 2$ is also implied and the new 3×2 Yukawa coupling matrices Y^m are

$$Y^{+2} = Y^{-2} = -Y^{+1} = Y^{-1} = Y^0 = \frac{1}{\sqrt{2}} [(x+z), i(z-x)]. \quad (13)$$

Including the SM Yukawa couplings

$$-\mathcal{L}_{\phi}^{\text{Yuk}} = (y_{\phi})_{ij} \overline{F}_{Li} \phi f_{Rj} + \text{h.c.}, \quad (14)$$

and a bare mass for Σ , the fermion mass terms read

$$-\mathcal{L}_m = \frac{1}{2} \overline{N}_L M_N N_R + \overline{E}_L M_E E_R + \overline{D}_L M_D D_R + \text{h.c.}, \quad (15)$$

where the mass matrices are

$$\begin{aligned} M_N &= \begin{pmatrix} 0_3 & (x+z)^* v_{\Phi} & i(x-z)^* v_{\Phi} \\ (x+z)^{\dagger} v_{\Phi} & M_{\Sigma} & 0 \\ i(x-z)^{\dagger} v_{\Phi} & 0 & M_{\Sigma} \end{pmatrix}, \\ M_E &= \begin{pmatrix} y_{\phi} v_{\phi} & \sqrt{3/2} (x+z)^* v_{\Phi} & i\sqrt{3/2} (x-z)^* v_{\Phi} \\ 0 & M_{\Sigma} & 0 \\ 0 & 0 & M_{\Sigma} \end{pmatrix}, \\ M_D &= M_{\Sigma} \mathbf{1}_2, \end{aligned} \quad (16)$$

in the basis

$$N_L = \begin{pmatrix} n_L \\ \Sigma_{1L}^0 \\ \Sigma_{2L}^0 \end{pmatrix}, \quad N_R = N_L^C, \quad E = \begin{pmatrix} f \\ \Sigma_1^- \\ \Sigma_2^- \end{pmatrix}, \quad D = \begin{pmatrix} \Sigma_1^{--} \\ \Sigma_2^{--} \end{pmatrix}. \quad (17)$$

1. Diagonalization of fermion mass matrices

As we will see later, the mixing between heavy and light charged particles is tiny, with negligible corrections to their mass eigenvalues. We first diagonalize the submatrix for light charged leptons by bi-unitary transformations, $F_L \rightarrow \mathcal{U}_L F_L$, $f_R \rightarrow \mathcal{U}_R f_R$, so that

$$\mathcal{U}_L^\dagger v_\phi y_\phi \mathcal{U}_R = \text{diag}(m_e, m_\mu, m_\tau). \quad (18)$$

The transformations will change nothing else in the Lagrangian but the Yukawa couplings,

$$\mathcal{U}_L^\dagger (x+z)^* = \frac{2\sqrt{3}r_\Phi}{v_\phi} \mathbf{u}_1, \quad \mathcal{U}_L^\dagger i(x-z)^* = \frac{2\sqrt{3}r_\Phi}{v_\phi} \mathbf{u}_2, \quad (19)$$

where $\mathbf{u}_{1,2}$ are two three-component column vectors which are determined by x , z , and \mathcal{U}_L . With the help of eq. (4), the mass matrices become

$$M_N = \begin{pmatrix} 0_3 & \kappa U \\ \kappa U^T & M_\Sigma \mathbf{1}_2 \end{pmatrix}, \quad M_E = \begin{pmatrix} \text{diag}(m_e, m_\mu, m_\tau) & \sqrt{3/2} \kappa U \\ 0 & M_\Sigma \mathbf{1}_2 \end{pmatrix}, \quad (20)$$

where $U = (\mathbf{u}_1, \mathbf{u}_2)$.

To diagonalize M_N , we first deal with the light-heavy mixing,

$$(U_N^{\text{l-h}})^\dagger M_N (U_N^{\text{l-h}})^* = \begin{pmatrix} M_{\text{light}}^\nu & \\ & M_\Sigma \mathbf{1}_2 \end{pmatrix}, \quad (21)$$

by

$$U_N^{\text{l-h}} = \begin{pmatrix} \mathbf{1}_3 - \kappa^2 \frac{UU^\dagger}{2M_\Sigma^2} & \kappa U / M_\Sigma \\ -\kappa U^\dagger / M_\Sigma & \mathbf{1}_2 - \kappa^2 \frac{U^\dagger U}{2M_\Sigma^2} \end{pmatrix}, \quad (22)$$

so that

$$M_{\text{light}}^\nu = -ZZ^T, \quad (23)$$

where $Z = (\mathbf{z}_1, \mathbf{z}_2)$ is a 3×2 matrix in terms of the column vectors $\mathbf{z}_{1,2} = \kappa \mathbf{u}_{1,2} / \sqrt{M_\Sigma}$. The matrix M_{light}^ν can be diagonalized by the PMNS matrix,

$$U_{\text{PMNS}}^\dagger M_{\text{light}}^\nu U_{\text{PMNS}}^* = \text{diag}(m_{\nu_1}, m_{\nu_2}, m_{\nu_3}), \quad (24)$$

with tiny corrections to the definition of U_{PMNS} from the heavy-light mixing of singly charged fermions. Now we employ an algebraic trick in Ref. [45] to solve Z in terms of U_{PMNS} , m_{ν_i} and

free physical parameters. Writing $U_{\text{PMNS}} = (\mathbf{x}_1, \mathbf{x}_2, \mathbf{x}_3)$ and noting that one of the light neutrinos is massless in the considered model [44], we can parameterize Z for normal hierarchy (NH) and inverted hierarchy (IH) of neutrino mass,

$$\begin{aligned}
\text{NH: } m_{\nu_1} &= 0, m_{\nu_2} = \lambda_-, m_{\nu_3} = \lambda_+, \\
\mathbf{z}_1 &= c_- \mathbf{x}_2 + c_+ \mathbf{x}_3, \mathbf{z}_2 = d_- \mathbf{x}_2 + d_+ \mathbf{x}_3, \\
\text{IH: } m_{\nu_3} &= 0, m_{\nu_1} = \lambda_-, m_{\nu_2} = \lambda_+, \\
\mathbf{z}_1 &= c_- \mathbf{x}_1 + c_+ \mathbf{x}_2, \mathbf{z}_2 = d_- \mathbf{x}_1 + d_+ \mathbf{x}_2,
\end{aligned} \tag{25}$$

where $\lambda_+ > \lambda_- > 0$ are the two non-zero mass eigenvalues. The coefficients c_{\pm}, d_{\pm} can be expressed in terms of the eigenvalues λ_{\pm} plus a free complex parameter t . For both hierarchies, we have

$$\begin{aligned}
c_- &= i\sqrt{\lambda_-} \frac{2t}{1+t^2}, \quad d_- = i\sqrt{\lambda_-} \frac{1-t^2}{1+t^2}, \\
c_+ &= i\sqrt{\lambda_+} \frac{1-t^2}{1+t^2}, \quad d_+ = -i\sqrt{\lambda_+} \frac{2t}{1+t^2}.
\end{aligned} \tag{26}$$

The preceding matrices can now be determined in terms of Z . For instance,

$$U = \frac{\sqrt{M_{\Sigma}}}{\kappa} Z, \tag{27}$$

and the complete transformation matrix for neutral fermions, $\nu_L = U_N^{\dagger} N_L$, $\nu_R = \nu_L^C$, reads

$$U_N = \begin{pmatrix} \left(\mathbf{1}_3 - \frac{ZZ^{\dagger}}{2M_{\Sigma}} \right) U_{\text{PMNS}} & \frac{Z}{\sqrt{M_{\Sigma}}} \\ -\frac{Z^{\dagger} U_{\text{PMNS}}}{\sqrt{M_{\Sigma}}} & \mathbf{1}_2 - \frac{1}{2M_{\Sigma}} Z^{\dagger} Z \end{pmatrix}. \tag{28}$$

The mass matrix M_E for singly charged fermions is diagonalized by bi-unitary transformation, $\ell_L = U_L^{\dagger} E_L$, $\ell_R = U_R^{\dagger} E_R$, to $M_{\ell} = \text{diag}(m_e, m_{\mu}, m_{\tau}, m_{\Sigma_1^-}, m_{\Sigma_2^-})$. U_L diagonalizes $M_E M_E^{\dagger}$, and is found in the limit of $M_{\Sigma} \gg m_{\tau}$, to be

$$U_L = \begin{pmatrix} \mathbf{1}_3 - \frac{3}{4M_{\Sigma}} ZZ^{\dagger} & \sqrt{\frac{3}{2M_{\Sigma}}} Z \\ -\sqrt{\frac{3}{2M_{\Sigma}}} Z^{\dagger} & \mathbf{1}_2 - \frac{3}{4M_{\Sigma}} Z^{\dagger} Z \end{pmatrix}. \tag{29}$$

Similarly, U_R diagonalizes $M_E^{\dagger} M_E$, and is found to be

$$U_R = \begin{pmatrix} \mathbf{1}_3 - \frac{3}{4}\eta\eta^{\dagger} & \sqrt{\frac{3}{2}}\eta \\ -\sqrt{\frac{3}{2}}\eta^{\dagger} & \mathbf{1}_2 - \frac{3}{4}\eta^{\dagger}\eta \end{pmatrix}, \tag{30}$$

with $\eta = M_\Sigma^{-3/2} \text{diag}(m_e, m_\mu, m_\tau)Z$. The mixing is suppressed by an additional factor of $m_{e,\mu,\tau}/M_\Sigma$ compared to U_L .

The above mixing matrices will enter into gauge interactions of the fermions as well as Yukawa couplings. In the basis of eq. (17), the weak and electromagnetic currents are

$$\begin{aligned} J_W^{+\mu} &= \bar{N}\gamma^\mu(w_L P_L + w_R P_R)E + 2\bar{E}\gamma^\mu w_D D, \\ J_Z^\mu &= \bar{N}\gamma^\mu z_L^N P_L N + \bar{E}\gamma^\mu(z_L^E P_L + z_R^E P_R)E - 2c_W^2 \bar{D}\gamma^\mu D, \\ J_{\text{em}}^\mu &= -\bar{E}\gamma^\mu E - 2\bar{D}\gamma^\mu D, \end{aligned} \quad (31)$$

where

$$\begin{aligned} w_L &= \begin{pmatrix} \mathbf{1}_3 & \\ & \sqrt{6}\mathbf{1}_2 \end{pmatrix}, \quad w_R = \begin{pmatrix} 0_3 & \\ & \sqrt{6}\mathbf{1}_2 \end{pmatrix}, \quad w_D = \begin{pmatrix} 0_{3 \times 2} \\ \mathbf{1}_2 \end{pmatrix}, \\ z_L^N &= \begin{pmatrix} \frac{1}{2}\mathbf{1}_3 & \\ & 0_2 \end{pmatrix}, \quad z_L^E = \begin{pmatrix} (-\frac{1}{2} + s_W^2)\mathbf{1}_3 & \\ & -c_W^2\mathbf{1}_2 \end{pmatrix}, \quad z_R^E = \begin{pmatrix} s_W^2\mathbf{1}_3 & \\ & -c_W^2\mathbf{1}_2 \end{pmatrix}. \end{aligned} \quad (32)$$

In terms of the mass eigenstates, they become

$$\begin{aligned} J_W^{+\mu} &= \bar{\nu}\gamma^\mu(\mathcal{W}_L P_L + \mathcal{W}_R P_R)\ell + 2\bar{\ell}\gamma^\mu(\mathcal{W}_L^D P_L + \mathcal{W}_R^D P_R)D, \\ J_Z^\mu &= \bar{\nu}\gamma^\mu \mathcal{Z}_L^\nu P_L \nu + \bar{\ell}\gamma^\mu(\mathcal{Z}_L^\ell P_L + \mathcal{Z}_R^\ell P_R)\ell - 2c_W^2 \bar{D}\gamma^\mu D, \\ J_{\text{em}}^\mu &= -\bar{\ell}\gamma^\mu \ell - 2\bar{D}\gamma^\mu D, \end{aligned} \quad (33)$$

where the matrices \mathcal{W}_L etc are given in Appendix A. As can be seen from there, the flavor changing neutral currents (FCNC) of the light charged leptons are suppressed by a factor of light neutrino mass over M_Σ for the left-handed chirality and by even an additional factor of light charged lepton mass over M_Σ for the right-handed chirality.

III. LEPTON FLAVOR VIOLATING TRANSITIONS

We will study the LHC production and detection of new particles in section IV. To make this realistic, we have to consider the constraints that are already available on the new interactions. As we will show in this section, the precise measurements in LFV transitions indeed set strong bounds on the relevant couplings.

Since the deviation from SM gauge interactions is significantly suppressed by a small mass ratio $\sqrt{m_\nu/M_\Sigma}$ or even more, we focus on the new Yukawa couplings. With the fields redefined in

eq. (11) and the transformations in eq. (19), the relevant Yukawa couplings are written as

$$-\mathcal{L}_{\Phi}^{\text{Yuk}} \supset \sum_{m=-2}^{+1} \sqrt{2-m} Y_{ix}^m \Phi_{m+1} \bar{\Sigma}_x^m P_L \ell_i + \text{h.c.}, \quad (34)$$

where now

$$Y^{-2} = Y^{-1} = Y^0 = -Y^{+1} = \frac{\sqrt{M_{\Sigma}}}{\sqrt{2}v_{\Phi}} Z^*, \quad (35)$$

and further mixing of the SM charged leptons ℓ_i can be safely ignored as we discussed in the last section.

A. Radiative transitions and electromagnetic dipole moments

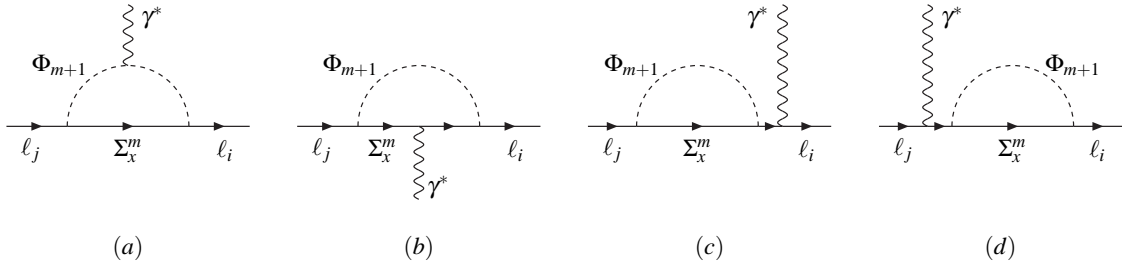


FIG. 1: Diagrams for radiative transitions.

The diagrams contributing to radiative transitions are shown in Fig. 1. Ignoring the mass splitting among Σ 's (and Φ 's) of various charges and working in the small mass limit of light charged leptons, a calculation similar to that in Ref. [45] yields the amplitude for the process $\ell_j(p) \rightarrow \ell_i(p-q)\gamma^*(q)$,

$$\begin{aligned} \mathcal{A}_{\mu}^m(\ell_j \rightarrow \ell_i \gamma^*) = & \frac{-e(ZZ^{\dagger})_{ij}}{2(4\pi)^2 v_{\Phi}^2 M_{\Sigma}} \bar{u}_i(p-q) \left[F_m(r) (P_R m_j + P_L m_i) i \sigma_{\mu\nu} q^{\nu} \right. \\ & \left. + G_m(r) P_R (q^2 \gamma_{\mu} - q q_{\mu}) \right] u_j(p), \end{aligned} \quad (36)$$

where $m = -2, \dots, +1$ refers to the charge of the virtual Σ^m in the loop, and the functions are

$$\begin{aligned} F_m(r) &= r(2-m)[(m+1)F^a(r) - mF^b(r)], \\ G_m(r) &= r(2-m)[(m+1)G^a(r) - mG^b(r)], \end{aligned} \quad (37)$$

with $r = M_{\Sigma}^2/M_{\Phi}^2$ and the functions $F^{a,b}$ and $G^{a,b}$ are given in Appendix B.

For on-shell transitions, only the dipole term survives and yields the branching ratio

$$\text{BR}(\ell_j \rightarrow \ell_i \gamma) = \text{BR}(\ell_j \rightarrow \ell_i \bar{\nu}_i \nu_j) \times \frac{3\alpha |(ZZ^\dagger)_{ij}|^2}{64\pi G_F^2 v_\Phi^4 M_\Sigma^2} \left[\sum_{m=-2}^1 F_m(r) \right]^2, \quad (38)$$

and the contribution to the anomalous magnetic moment of ℓ_i is obtained as a by-product,

$$a(\ell_i) = \frac{m_i^2 (ZZ^\dagger)_{ii}}{(4\pi)^2 v_\Phi^2 M_\Sigma} \sum_{m=-2}^1 F_m(r). \quad (39)$$

B. Purely leptonic decays

With three generations of SM leptons, there are three possible types of purely leptonic transitions:

$$\begin{aligned} (1) \quad & \ell_l(p) \rightarrow \ell_i(k_1) \ell_i(k_2) \bar{\ell}_k(k_3), \quad \ell_i \neq \ell_k, \\ (2) \quad & \ell_l(p) \rightarrow \ell_i(k_1) \ell_j(k_2) \bar{\ell}_j(k_3), \quad \ell_i \neq \ell_j, \\ (3) \quad & \ell_l(p) \rightarrow \ell_i(k_1) \ell_i(k_2) \bar{\ell}_i(k_3). \end{aligned} \quad (40)$$

As we discussed at the end of sec II, FCNC at tree level contributes little to the transitions because of strong suppression in both chiralities. We thus focus on the loop contributions due to new Yukawa couplings. The calculation is again similar to that in Ref. [45] for the color-octet model.

The type-(1) decay is contributed only by the box diagram in Fig. 2,

$$\mathcal{A}^m(1) = \frac{-(ZZ^\dagger)_{il}(ZZ^\dagger)_{ik}}{2(4\pi)^2 v_\Phi^4} [\bar{u}(k_1) \gamma_\mu P_L u(p)] [\bar{u}(k_2) \gamma^\mu P_L v(k_3)] H_m(r), \quad (41)$$

where a factor of 2 has been attached since the two minus signs from identical fermions in the final state and from the Fierz identity cancel each other, and $H_m(r) = (2-m)^2 H(r)$ with $H(r)$ given in Appendix B. A summation over the fermion charge m is always implied in the amplitude.

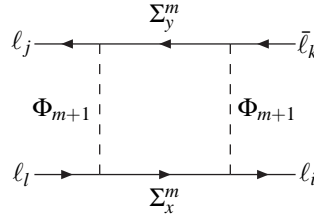


FIG. 2: Additional box diagram for purely leptonic transitions.

For type-(2) decay, both radiative and box diagrams contribute,

$$\mathcal{A}^m(2) = \mathcal{A}_\Delta^m + \mathcal{A}_\square^m, \quad (42)$$

where

$$\begin{aligned} \mathcal{A}_\Delta^m &= \frac{\alpha(ZZ^\dagger)_{il}}{8\pi v_\Phi^2 M_\Sigma} \bar{u}(k_2) \gamma^\mu v(k_3) \\ &\quad \times \bar{u}(k_1) \left[F_m(r) (P_R m_l + P_L m_i) i\sigma_{\mu\nu} (k_2 + k_3)^\nu s_{23}^{-1} + G_m(r) P_R \gamma_\mu \right] u(p), \\ \mathcal{A}_\square^m &= \frac{-1}{4(4\pi)^2 v_\Phi^4} \left[(ZZ^\dagger)_{il} (ZZ^\dagger)_{jj} + (ZZ^\dagger)_{jl} (ZZ^\dagger)_{ij} \right] \\ &\quad \times \bar{u}(k_2) \gamma^\mu P_L v(k_3) \bar{u}(k_1) \gamma_\mu P_L u(p) H_m(r), \end{aligned} \quad (43)$$

with $s_{ij} = (k_i + k_j)^2$. Finally, the type-(3) decay arises as a special case of type-(2), with all leptons in the final state of the same flavor,

$$\mathcal{A}^m(3) = \mathcal{A}^m(2)|_{j=i} - (k_1 \leftrightarrow k_2). \quad (44)$$

The branching ratios for all three types of decays are worked out using the phase space integrals computed in Ref. [45] to be,

$$\text{BR}(1) = \text{BR}(\ell_l \rightarrow \ell_i \nu_l \bar{\nu}_i) \frac{|(ZZ^\dagger)_{il} (ZZ^\dagger)_{ik}|^2}{2^{14} \pi^4 v_\Phi^8 G_F^2} \left[\sum_{m=-2}^1 H_m(r) \right]^2, \quad (45)$$

$$\begin{aligned} \text{BR}(2) &= \text{BR}(\ell_l \rightarrow \ell_i \nu_l \bar{\nu}_i) \frac{1}{2^{13} \pi^4 v_\Phi^4 G_F^2} \left\{ \left| \sum_m (B^m + T_1^m) \right|^2 + \left| \sum_m T_1^m \right|^2 \right. \\ &\quad \left. - 4\text{Re} \left(\sum_m B^m T_2^{m*} \right) - 8\text{Re} \left(\sum_m T_1^m T_2^{m*} \right) + \left[-\frac{14}{3} + 8 \ln \frac{m_l^2}{4m_i^2} \right] \left| \sum_m T_2^m \right|^2 \right\}, \end{aligned} \quad (46)$$

$$\begin{aligned} \text{BR}(3) &= \text{BR}(\ell_l \rightarrow \ell_i \nu_l \bar{\nu}_i) \frac{1}{2^{13} \pi^4 v_\Phi^4 G_F^2} \left\{ 2 \left| \sum_m (B^m + T_1^m) \right|^2 + \left| \sum_m T_1^m \right|^2 \right. \\ &\quad \left. - 8\text{Re} \left(\sum_m B^m T_2^{m*} \right) - 12\text{Re} \left(\sum_m T_1^m T_2^{m*} \right) + \left[-\frac{8}{3} + 8 \ln \frac{m_l^2}{4m_i^2} \right] \left| \sum_m T_2^m \right|^2 \right\}, \end{aligned} \quad (47)$$

where for type-(2) decay,

$$\begin{aligned} B^m &= -\frac{1}{2v_\Phi^2} \left[(ZZ^\dagger)_{il} (ZZ^\dagger)_{jj} + (ZZ^\dagger)_{jl} (ZZ^\dagger)_{ij} \right] H_m(r), \\ T_1^m &= \frac{e^2 (ZZ^\dagger)_{il}}{M_\Sigma} G_m(r), \\ T_2^m &= \frac{e^2 (ZZ^\dagger)_{il}}{M_\Sigma} F_m(r), \end{aligned} \quad (48)$$

and for type-(3) decay $j = i$ is set in the above functions.

We note incidentally that the amplitude for the type-(1) decay also implies the effective interaction for muonium-anti-muonium oscillation:

$$\mathcal{L}_{\text{eff}} = -G_{M\bar{M}} \bar{\mu} \gamma^\alpha P_L e \mu \gamma_\alpha P_L e, \quad (49)$$

where the effective Fermi constant is,

$$\frac{G_{M\bar{M}}}{\sqrt{2}} = \frac{[(ZZ^\dagger)_{\mu e}]^2}{4(4\pi)^2 v_\Phi^4} \sum_m H_m(r). \quad (50)$$

C. $\mu - e$ conversion in nuclei

Our result in the previous subsections can also be applied to the $\mu - e$ conversion in nuclei. The effective Lagrangian can be written as

$$-\mathcal{L}_{\mu e} = \frac{4}{\sqrt{2}} (m_\mu A_R \bar{e} P_R \sigma^{\mu\nu} \mu F_{\mu\nu} + \text{h.c.}) + \frac{1}{\sqrt{2}} \sum_{q=u,d,s} (g_{LV(q)} \bar{e} \gamma^\mu P_L \mu \bar{q} \gamma_\mu q + \text{h.c.}), \quad (51)$$

where $F_{\mu\nu}$ is the electromagnetic field strength and the effective couplings are

$$\begin{aligned} A_R &= \frac{\sqrt{2} e (ZZ^\dagger)_{e\mu}}{16(4\pi)^2 v_\Phi^2 M_\Sigma} \sum_m F_m(r), \\ g_{LV(u)} &= \frac{2}{3} \frac{\alpha (ZZ^\dagger)_{e\mu}}{\sqrt{2} (4\pi) v_\Phi^2 M_\Sigma} \sum_m G_m(r), \\ g_{LV(d,s)} &= -\frac{1}{3} \frac{\alpha (ZZ^\dagger)_{e\mu}}{\sqrt{2} (4\pi) v_\Phi^2 M_\Sigma} \sum_m G_m(r). \end{aligned} \quad (52)$$

Then the $\mu - e$ conversion branching ratio is given by [46]

$$\text{BR}(\mu^- N \rightarrow e^- N) = \frac{2|A_R D + \tilde{g}_{LV}^{(p)} V^{(p)} + \tilde{g}_{LV}^{(n)} V^{(n)}|^2}{\omega_{\text{capt}}}, \quad (53)$$

where

$$\begin{aligned} \tilde{g}_{LV}^{(p)} &= 2g_{LV(u)} + g_{LV(d)} = \frac{\alpha (ZZ^\dagger)_{e\mu}}{\sqrt{2} (4\pi) v_\Phi^2 M_\Sigma} \sum_m G_m(r), \\ \tilde{g}_{LV}^{(n)} &= g_{LV(u)} + 2g_{LV(d)} = 0, \end{aligned} \quad (54)$$

and D , $V^{(p)}$ and $V^{(n)}$ are overlap integrals which are numerically evaluated together with the corresponding ordinary muon capture rate ω_{capt} [46].

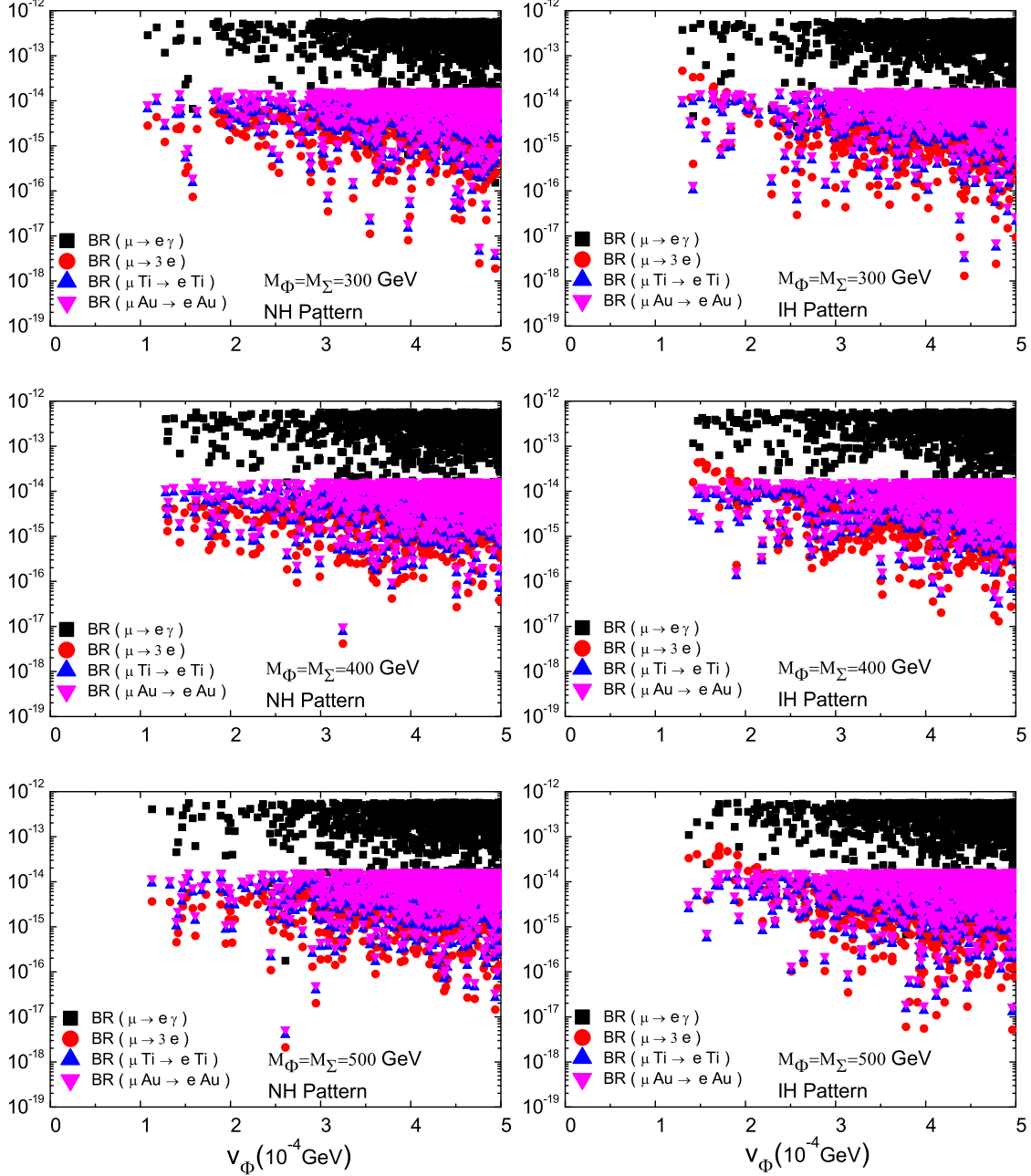


FIG. 3: Points allowed by current bounds on LFV transitions are shown for $M_\Phi = M_\Sigma = 300, 400, 500$ GeV and for NH and IH patterns in the small VEV range $v_\Phi \lesssim 5 \times 10^{-4}$ GeV.

The most stringent upper bound on the radiative LFV decays comes from $\text{BR}(\mu \rightarrow e\gamma) < 5.7 \times 10^{-13}$ (90% C.L.) [47]. Concerning the pure leptonic decays, the record is still held by the old result $\text{BR}(\mu \rightarrow 3e) < 1.0 \times 10^{-12}$ (90% C.L.) [48]. The current bound on $\mu - e$ conversion in nuclei also looks competitive, $\text{BR}(\mu^- \text{Ti} \rightarrow e^- \text{Ti}) < 4.3 \times 10^{-12}$ (90% C.L.) and $\text{BR}(\mu^- \text{Au} \rightarrow e^- \text{Au}) < 7 \times 10^{-13}$ (90% C.L.) [49], while the current bound on the muonium-

antimuonium oscillation, $G_{M\bar{M}} \leq 3.0 \times 10^{-3} G_F$ (90% C.L.) [50] is still too poor to be useful. Using the analytical results in this section, we have made a numerical scanning on the parameter regions that respect the above experimental bounds and are potentially accessible at LHC.

The most relevant parameters for our later analysis of the LHC phenomenology are the masses $M_{\Sigma, \Phi}$ of the new particles and the VEV v_Φ . As usual, a larger mass tends to suppress the LFV transitions. We scan parameters for relatively light, degenerate new particles that would be accessible at LHC, i.e., $M_\Sigma = M_\Phi = 300, 400, 500$ GeV. Similarly, since a larger v_Φ implies smaller Yukawa couplings and is thus safe for LFV transitions, we scan it in the range of smaller values, $v_\Phi \lesssim 5 \times 10^{-4}$ GeV. This is also the range in which the like-sign dilepton signals are important at LHC. We allow the neutrino mass squared differences and mixing angles to assume a random value in their 3σ ranges, set the unknown CP phases to zero and the parameter t to take a value randomly. Then, the matrix Z is fully determined by eqs. (25) and (26) for both hierarchy patterns, and the branching ratios for the decays $\mu \rightarrow e\gamma$, $3e$ and the $\mu - e$ conversion in nuclei can be evaluated with the help of eqs. (38), (47), and (53). The scanning results passing all constraints are shown in Fig. 3.

As one can see from Fig. 3, the current bound on $\text{BR}(\mu \rightarrow e\gamma)$ sets the most stringent constraint. Respecting it implies that all other LFV transitions are well below their current bounds. The allowed lower bound on the VEV is about $v_\Phi \sim O(10^{-4})$ GeV. Generally speaking, the bound should increase with heavy masses, though this is not very obvious in Fig. 3. This is partly because the three values chosen for the masses are too close and partly because of fluctuations in sampling the parameters with a limited number of points. This does not affect our interest in a small v_Φ at LHC when the like-sign dilepton signals are relevant. We will thus assume $v_\Phi = 10^{-4}$ GeV for the purpose of illustration. Since the light neutrino masses (and thus elements in Z) in the IH case are larger than in the NH case, the lower bound on v_Φ in the IH case is a bit larger. Finally, we note in passing that this lower bound on the scalar VEV from LFV transitions is much stronger than in the type II seesaw, see for example, Ref. [51]. The reason for this difference is clear. Our neutrino mass arises from a dimension-nine operator, resulting in $m_\nu \sim (v_\Phi^2/M_\Sigma)YY^\dagger$ [44], while it is from a dimension-five operator in the latter case with $m_\nu \sim v_\Delta Y$, where v_Δ is the triplet VEV. For given m_ν and assuming a similar mass for all heavy particles, the LFV upper bounds on Y translate roughly into a relation between the lower bounds on the VEV's, $v_\Phi \sim v_\Delta (M_\Sigma/m_\nu)^{1/2}$.

IV. COLLIDER PHENOMENOLOGY OF CASCADE SEESAW MODEL

We explore in this section the collider signatures of the minimal version of the cascade seesaw detailed in the last section. Our analysis procedure is as follows. We implement the model in the *Mathematica* package FeynRules1.7 [52], whose output UFO model file is taken by Madgraph5 [53] to generate the parton level events for the relevant physical processes. Those events then pass through Pythia6 [54] to include the initial- and final-state radiation, fragmentation, and hadronization. We use PGS for the detector simulation and MadAnalysis5 [55] for the analysis. In our simulation, we employ the CTEQ6L1 parton distribution function (PDF) [56]. Concerning the physical parameters, we recall that, using our parametrization, all mixing matrices are expressed in terms of the two free parameters, the quadruplet VEV v_Φ and the complex parameter t . Together with the masses of the new particles, M_Φ and M_Σ , all production rates and decay widths are fixed. And to simplify the matter, we assume that the scalars (fermions) of various charges are degenerate. However, it is straightforward to include the non-degenerate case in our code and we will leave this general case for another work. The constraints from low energy processes are respected in our analysis of collider phenomenology, which allows us to set comprehensive bounds on the model in the future. For the purpose of illustration, we often work with the benchmark parameter points, $M_\Phi = M_\Sigma = 300$ GeV, $t = 1 + i$, and $v_\Phi = 10^{-4}$ or 10^{-2} GeV. Our numerical results are not particularly sensitive to the t parameter except at the singular points $t = \pm i$ where our parametrization (26) is not appropriate. For instance, LFV transitions are not affected by its magnitude being larger or small than unity because the transformation $t \rightarrow -t^{-1}$ only flips the global sign of the matrix Z [45].

The new physical particles in our model are, the scalar quadruplet which includes as its members the neutral CP-even (-odd) H_0 (A_0), the singly charged Φ_{-1}/Φ_{-1}^* , Φ_{+1}/Φ_{+1}^* , and the doubly charged Φ_{+2}/Φ_{+2}^* , and the fermion quintuplet which includes the neutral Σ^0 , the singly charged Σ^\pm , and the doubly charged $\Sigma^{\pm\pm}$ particles. The dominant production of these particles at hadron colliders proceeds via the Drell-Yan process through an s-channel exchange of a photon and Z boson for the pair production,

$$\begin{aligned} pp &\rightarrow \gamma^*/Z^* \rightarrow \Phi_{+2}^*\Phi_{+2}/\Phi_{+1}^*\Phi_{+1}/\Phi_{-1}^*\Phi_{-1}/A_0H_0, \\ &\rightarrow \gamma^*/Z^* \rightarrow \Sigma^{++}\Sigma^{--}/\Sigma^+\Sigma^-, \end{aligned} \tag{55}$$

or of a W boson for the associated production,

$$\begin{aligned} pp &\rightarrow W^* \rightarrow \Phi_{+1}^* \Phi_{+2} / A_0 \Phi_{+1} / A_0 \Phi_{-1}^* / H_0 \Phi_{+1} / H_0 \Phi_{-1}^*, \\ &\rightarrow W^* \rightarrow \Sigma^{++} \Sigma^- / \Sigma^+ \Sigma^0, \end{aligned} \quad (56)$$

plus their charge conjugates. The subdominant channels involving h , A_0 , H_0 , Φ_{-1}^* , and Φ_{+1} exchanges and the vector boson fusion process with two extra jets [34] have much smaller cross sections and can be neglected.¹

In Fig. 4, the total cross section for various channels at LHC is plotted as a function of the masses $M_{\Phi, \Sigma}$. These channels have sizable rates, as they do not suffer from small mixing suppression. For instance, at LHC 14 TeV, the cross section is larger than 0.01 fb (1 fb) in each Φ (Σ) production channel up to a heavy mass of order 1 TeV. Nevertheless, to see whether it is really feasible to observe those new particles, we have to examine their decay properties and employ them to devise appropriate kinematical cuts to suppress the SM background.

A. Decay properties of new particles

In this subsection we study the decays of new particles in the minimal cascade seesaw model. All relevant decay widths are listed in Appendix C. As we stated earlier we assume for simplicity a degenerate spectrum for both the scalar quadruplet and the fermion quintuplet. Then, all new particles decay directly into the SM particles. For the four free parameters M_Φ , M_Σ , v_Φ and t , we evaluate at the benchmark points unless otherwise stated. In particular, $t = 1 + i$ is always assumed.

1. Doubly charged scalar Φ_{+2} decays

There are two decay modes for the doubly charged scalars, the lepton number violating (LNV) like-sign dilepton decays $\Phi_{+2} \rightarrow \ell_i^+ \ell_j^+$ ($\ell = e, \mu, \tau$) and the like-sign di- W decay $\Phi_{+2} \rightarrow W^+ W^+$. The amplitude for the former is proportional to the Yukawa coupling matrix for neutrinos and

¹ In this paper, we only consider the tree-level contributions. The QCD correction to doubly charged scalar pair production was computed in [57], with a K -factor of about 1.25, while the contribution from real photon annihilation tends to increase the production by 10%, resulting in an overall K -factor of 1.35 [11]. The associated production of scalars in principle gives a similar K -factor $\simeq 1.25$ [12]. However, to our knowledge, the similar study is missing for heavy fermions.

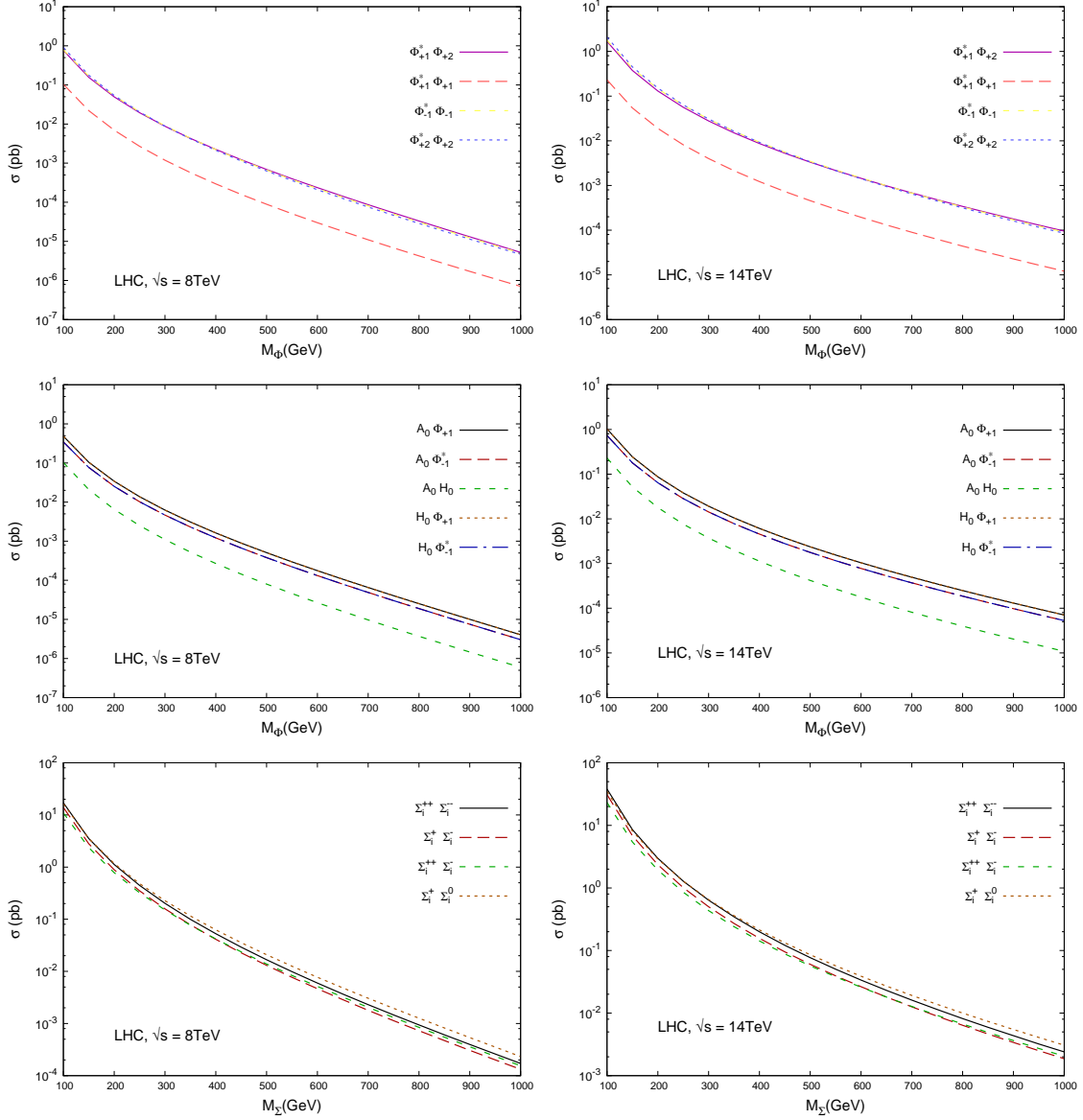


FIG. 4: Total cross section for various channels at LHC 8 TeV (14 TeV) is shown as a function of the mass M_Φ or M_Σ on the left (right) panel.

inversely proportional to v_Φ while the amplitude for the latter is proportional to v_Φ . The ratio between the two decay widths is given by

$$\frac{\Gamma(\Phi_{+2} \rightarrow \ell_i^+ \ell_j^+)}{\Gamma(\Phi_{+2} \rightarrow W^+ W^+)} \simeq \frac{|(ZZ^\dagger)_{ij}|^2 v_\phi^4}{M_\Phi^2 v_\Phi^4} \sim \left(\frac{m_\nu}{M_\Phi}\right)^2 \left(\frac{v_\phi}{v_\Phi}\right)^4. \quad (57)$$

The branching ratios are presented in Fig. 5. In the left panel, $\text{BR}(\Phi_{+2})$ is plotted as a function of v_Φ at $M_\Phi = 300$ GeV, while in the right panel it is plotted as a function of M_Φ at $v_\Phi = 10^{-4}$ GeV. From Fig. 5 and eq. (57), one finds that the two decay modes are comparable at, for instance,

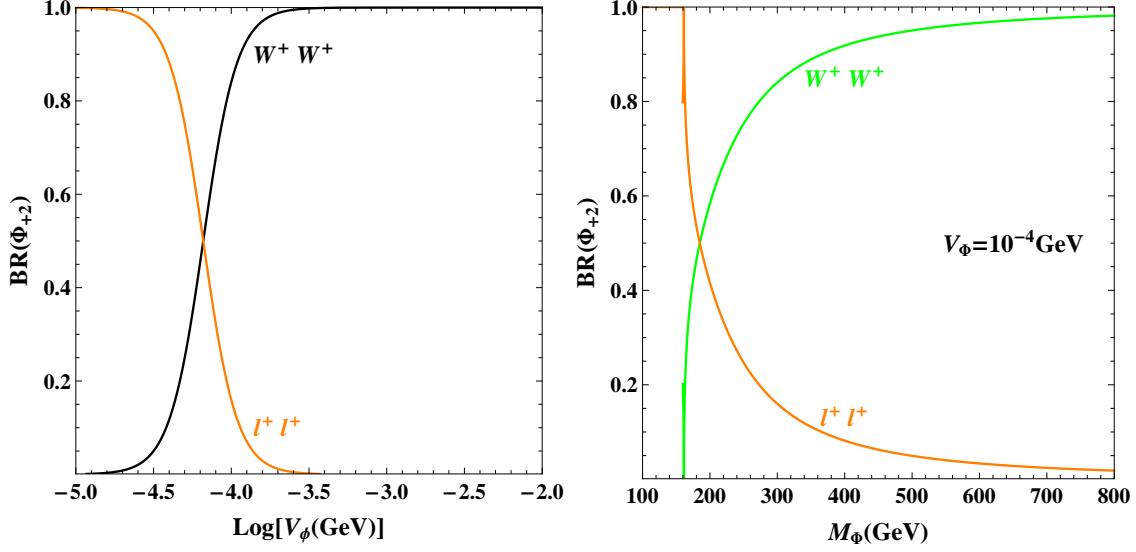


FIG. 5: Branching ratios of Φ_{+2} as a function of v_ϕ for $M_\Phi = 300$ GeV (left panel) and of M_Φ for $v_\phi = 10^{-4}$ GeV (right).

$v_\phi \sim 10^{-4}$ GeV and $M_\Phi \sim 200$ GeV. For a given M_Φ , the di- W decay dominates at a larger v_ϕ while the dilepton decay dominates at a smaller v_ϕ . As we discussed in section III, $v_\phi \approx 10^{-4}$ GeV is almost the lower bound allowed by the LFV transitions and thus the like-sign dilepton decay is suppressed in the majority of the parameter space. This sets a stringent constraint on the LHC search for doubly charged scalars in the dilepton channel. We will discuss this issue in more detail in subsection IV B.

2. Singly charged scalar Φ_{+1} and Φ_{-1} decays

The decay modes of the singly charged scalars Φ_{+1} and Φ_{-1} are similar except that $\Phi_{+1} \rightarrow ZW^+$ is absent. This difference arises from the mixing between the doublet and quadruplet scalars due to vacuum expectation values, so that Φ_{+1} does not couple to W^-Z . The decay amplitudes for $\Phi_{\pm 1} \rightarrow tb$, hW^\pm and $\Phi_{-1} \rightarrow ZW^-$ are proportional to v_ϕ , while those for $\Phi_{\pm 1} \rightarrow \ell_i^\pm \nu_j$ are proportional to the Yukawa coupling of neutrinos. In the left panel of Fig. 6, the relevant branching ratios are shown as a function of v_ϕ at $M_{\Phi_{\pm 1}} = 300$ GeV, and in the right panel as a function of $M_{\Phi_{\pm 1}}$ at $v_\phi = 10^{-2}$ GeV. For large values of v_ϕ , the important channels are $\Phi_{\pm 1} \rightarrow tb$, hW^\pm and $\Phi_{-1} \rightarrow ZW^-$, while $\Phi_{\pm 1} \rightarrow \ell_i^\pm \nu_j$ dominate for small v_ϕ and low M_Φ . Moreover, the decays $\Phi_{\pm 1} \rightarrow hW^\pm$ quickly dominate over $\Phi_{\pm 1} \rightarrow tb$ once M_Φ is slightly above the threshold for hW^\pm ,

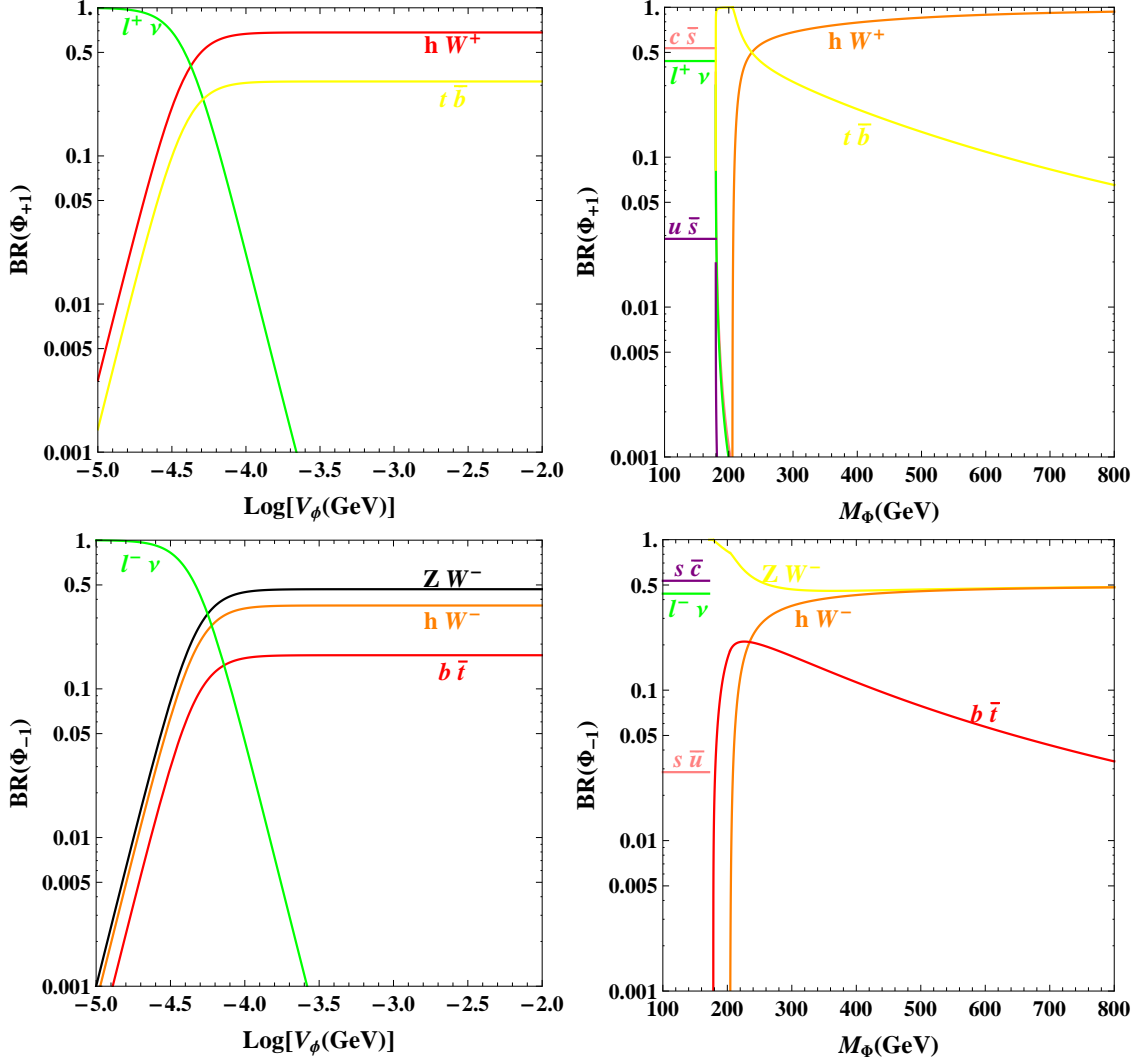


FIG. 6: Branching ratios of Φ_{+1} (upper panel) and Φ_{-1} (lower) as a function of v_ϕ for $M_\Phi = 300$ GeV (left panel) and of M_Φ for $v_\phi = 10^{-2}$ GeV (right).

while the decay width for $\Phi_{-1} \rightarrow ZW^-$ is always larger than for $\Phi_{-1} \rightarrow \bar{t}b$.

3. CP-even scalar H_0 and CP-odd scalar A_0 decays

The branching ratios for the neutral scalar decays are shown in Fig. 7. The relevant decay modes are, $H_0 \rightarrow W^+W^-, hh, ZZ, b\bar{b}, t\bar{t}$ and $A_0 \rightarrow hZ, b\bar{b}, t\bar{t}$, which are proportional to v_ϕ , and $H_0, A_0 \rightarrow \ell_i^+ \ell_j^-, \nu_i \nu_j$ which are proportional to the Yukawa coupling of neutrinos. For large v_ϕ , $H_0 \rightarrow hh, W^+W^-$ and $A_0 \rightarrow hZ$ are the dominant channels while $H_0 \rightarrow ZZ$ is relatively suppressed. The latter is in contrast to the usual type II seesaw model where the neutral member of the scalar

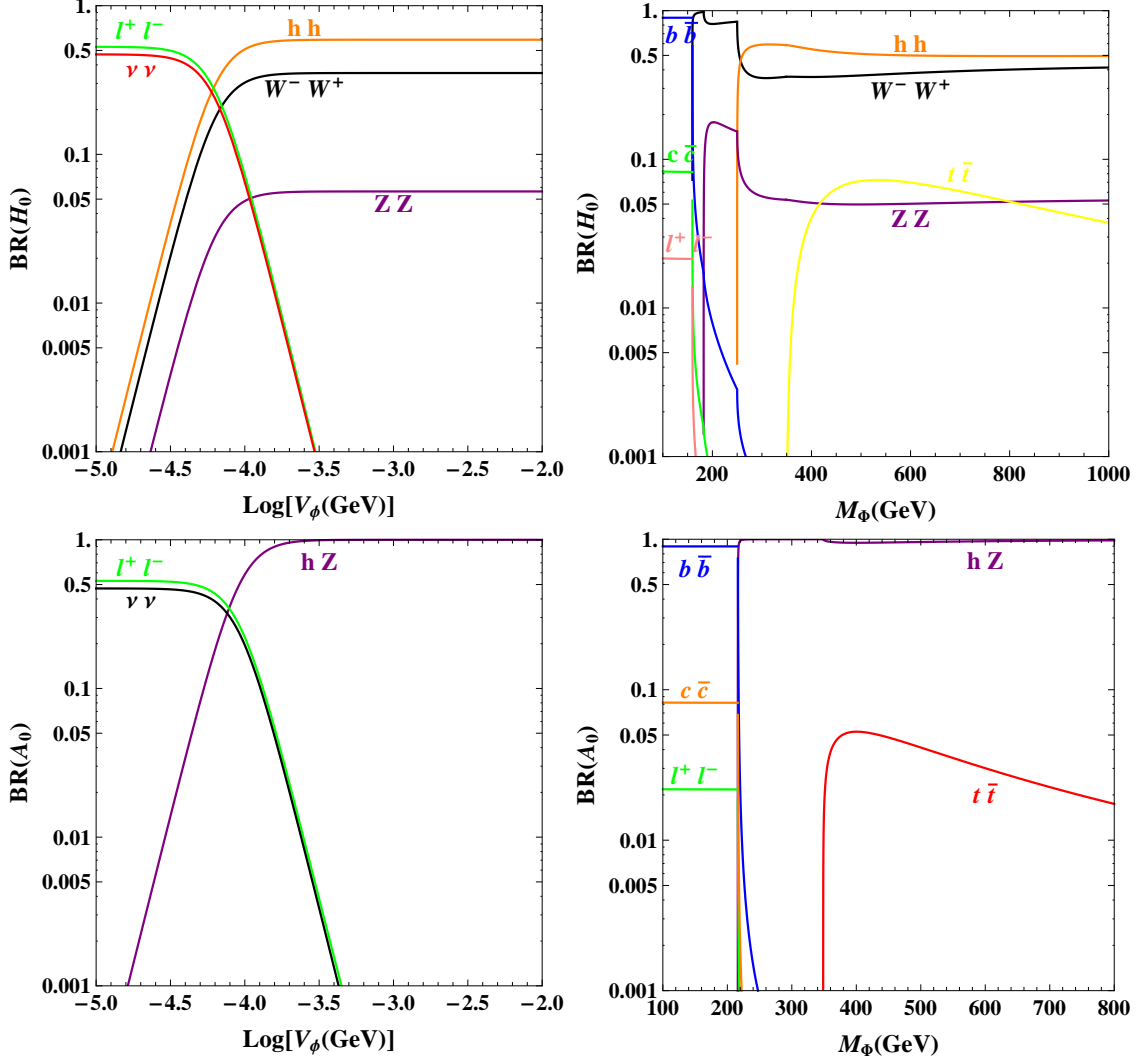


FIG. 7: Branching ratios of H_0 (upper panel) and A_0 (lower) as a function of v_ϕ for $M_\phi = 300$ GeV (left panel) and of M_ϕ for $v_\phi = 10^{-2}$ GeV (right).

triplet decays dominantly to a Z pair [12]. This again arises from different scalar mixing patterns in the two seesaw models. In the small v_ϕ region, the channels $H_0, A_0 \rightarrow \ell_i^+ \ell_j^-$, $\nu_i \nu_j$ become important. Due to the constraints from the low energy LFV processes, we will work at the two benchmark points in our signal analysis to demonstrate different features of the parameter space: $v_\phi = 10^{-4}$ GeV for the signal channels involving LNV dilepton decays, and $v_\phi = 10^{-2}$ GeV for other channels.

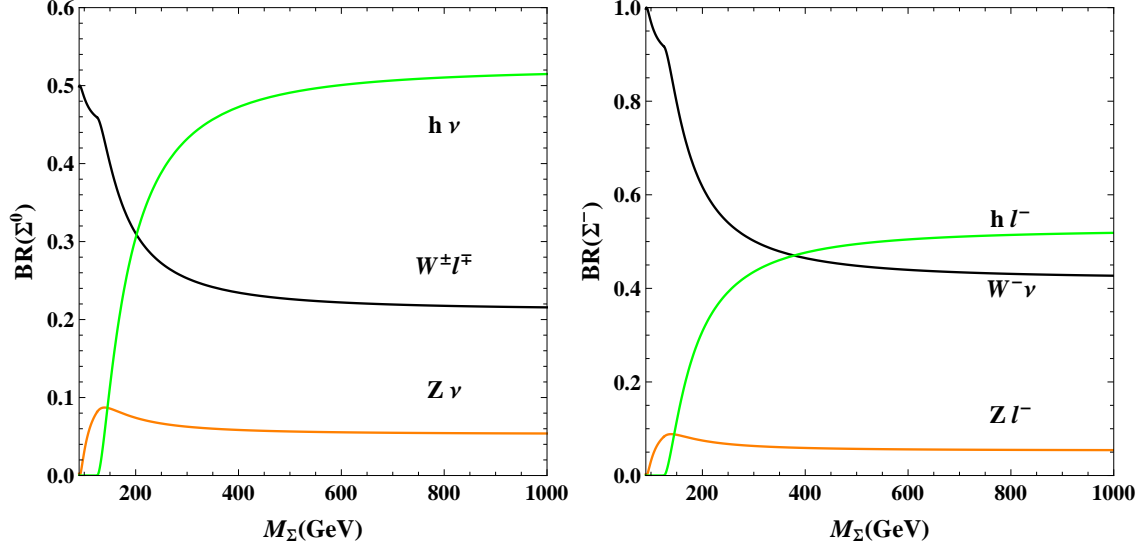


FIG. 8: Branching ratios of heavy fermions as a function of M_Σ .

4. Heavy quintuplet fermion decays

The most relevant decay channels of the quintuplet fermions are, $\Sigma^0 \rightarrow W^\pm \ell^\mp$, $h\nu$, $Z\nu$, and $\Sigma^- \rightarrow Z\ell^-$, $h\ell^-$, $W^-\nu$. In Fig. 8, we show the branching ratios for these channels versus the heavy fermion mass upon summing over the lepton flavors in the final states. The results for Σ^{--} are not presented since it has only one important decay, $\Sigma^{--} \rightarrow W^-\ell^-$. For lepton-flavor specific final states, $\ell = e, \mu, \tau$, we observe the following relations,

$$\begin{aligned} \text{BR}(\Sigma^0 \rightarrow W^\pm e^\mp) &> \text{BR}(\Sigma^0 \rightarrow W^\pm \mu^\mp) \approx \text{BR}(\Sigma^0 \rightarrow W^\pm \tau^\mp), \\ \text{BR}(\Sigma^- \rightarrow h e^-, Z e^-) &> \text{BR}(\Sigma^- \rightarrow h \mu^-, Z \mu^-) \approx \text{BR}(\Sigma^- \rightarrow h \tau^-, Z \tau^-), \\ \text{BR}(\Sigma^{--} \rightarrow W^- e^-) &> \text{BR}(\Sigma^{--} \rightarrow W^- \mu^-) \approx \text{BR}(\Sigma^{--} \rightarrow W^- \tau^-), \end{aligned} \quad (58)$$

for inverted neutrino mass hierarchy (IH), and

$$\begin{aligned} \text{BR}(\Sigma^0 \rightarrow W^\pm \mu^\mp) &\approx \text{BR}(\Sigma^0 \rightarrow W^\pm \tau^\mp) \gg \text{BR}(\Sigma^0 \rightarrow W^\pm e^\mp), \\ \text{BR}(\Sigma^- \rightarrow h \mu^-, Z \mu^-) &\approx \text{BR}(\Sigma^- \rightarrow h \tau^-, Z \tau^-) \gg \text{BR}(\Sigma^- \rightarrow h e^-, Z e^-), \\ \text{BR}(\Sigma^{--} \rightarrow W^- \mu^-) &\approx \text{BR}(\Sigma^{--} \rightarrow W^- \tau^-) \gg \text{BR}(\Sigma^{--} \rightarrow W^- e^-), \end{aligned} \quad (59)$$

for normal hierarchy (NH). Similar relations are also found in the usual type III seesaw model and can be understood as a consequence of the neutrino masses and mixing [16]. The well-separated neutrino mass squared differences Δm_{21}^2 and $|\Delta m_{23}^2|$ indicate that the branching ratios to specific

final states can differ by a few times in the IH case and by an order of magnitude in the NH case. This sensitivity to the mass hierarchy is considerably smeared out when summing over the lepton flavors in the final states. We therefore do not distinguish between the IH and NH cases in Fig. 8.

B. Signals of new particles at the LHC

In this subsection we study the experimental signatures of new particles at the LHC. We notice first that particles of equal charges appear also in the type II and III seesaw models. In applying the LHC search results one must be careful since those particles have generally different production and decay properties in different theoretical settings. For instance, both CMS and ATLAS experiments set a lower bound on the doubly charged scalars ranging from 204 GeV to 459 GeV [19] or from 375 GeV to 409 GeV [22], assuming that they decay exclusively into like-sign dileptons in the setting of type II seesaw. These bounds obviously do not apply to our case under consideration since the branching ratio of $\Phi^{\pm\pm} \rightarrow \ell^\pm \ell^\pm$ can never get close to 100% in the majority of the parameter space due to the constraints from low-energy LFV transitions. Similarly, both CMS [23] and ATLAS [24] have searched for pair production of heavy leptons in type III seesaw, and set a lower bound on their mass to be in the range 180 GeV to 210 GeV or 245 GeV respectively, assuming various patterns for the heavy-light lepton mixing.

There are many possible final states resulting from Φ and Σ production, given by the decay channels which we have discussed in subsection IV A. In Tables I and II, we collect the most relevant decay modes before including the sequential decays of SM particles. These channels lead to various signatures which are conventionally classified according to the multiplicity of the charged leptons. We consider the following seven signal channels:

- $2\ell^\pm 2\ell^\mp$, $2\ell^\pm 4j$ and $2\ell^\pm 4j + \cancel{E_T}$ channels from Φ production,
- $2\ell^\pm 2\ell^\mp 2j$, $3\ell^\pm \ell^\mp 2j$, $3\ell^\pm 2\ell^\mp \cancel{E_T}$ and $3\ell^\pm 3\ell^\mp$ channels from Σ production.

For clarity, we list all relevant final states and corresponding processes in Table III. They will be analyzed in detail in subsections IV B 1-IV B 7.

Before studying the simulation and analysis of signal channels, we estimate the signal events using the production cross sections and branching ratios discussed in the previous subsection. The number of signal events can be formally written as

$$N = L \times \text{production cross section} \times \text{decay branching ratios} \quad (60)$$

	$\Phi_{+1}^* \rightarrow b\bar{t} \text{ (0.32)}$	$\Phi_{+1}^* \rightarrow hW^- \text{ (0.68)}$	$\Phi_{-1}^* \rightarrow hW^+ \text{ (0.36)}$	$\Phi_{-1}^* \rightarrow ZW^+ \text{ (0.47)}$
$\Phi_{+1} \rightarrow t\bar{b} \text{ (0.32)}$	$b\bar{b}t\bar{t} \text{ (0.10)}$	$t\bar{b}hW^- \text{ (0.22)}$	—	—
$\Phi_{+1} \rightarrow hW^+ \text{ (0.68)}$	$b\bar{t}hW^+ \text{ (0.22)}$	$hhW^+W^- \text{ (0.47)}$	—	—
$\Phi_{-1} \rightarrow hW^- \text{ (0.36)}$	—	—	$hhW^+W^- \text{ (0.13)}$	$hZW^+W^- \text{ (0.17)}$
$\Phi_{-1} \rightarrow ZW^- \text{ (0.47)}$	—	—	$hZW^+W^- \text{ (0.17)}$	$hhW^+W^- \text{ (0.22)}$
$A_0 \rightarrow hZ \text{ (1.0)}$	—	—	$hhZW^+ \text{ (0.36)}$	$hZZW^+ \text{ (0.47)}$
$H_0 \rightarrow W^+W^- \text{ (0.35)}$	—	—	$hW^-W^+W^+ \text{ (0.13)}$	$ZW^-W^+W^+ \text{ (0.17)}$
$H_0 \rightarrow hh \text{ (0.60)}$	—	—	$hhhW^+ \text{ (0.22)}$	$hhZW^+ \text{ (0.28)}$
$\Phi_{+2} \rightarrow W^+W^+ \text{ (1.0)}$	$b\bar{t}W^+W^+ \text{ (0.32)}$	$hW^-W^+W^+ \text{ (0.68)}$	—	—
	$A_0 \rightarrow hZ \text{ (1.0)}$	$H_0 \rightarrow W^+W^- \text{ (0.35)}$	$H_0 \rightarrow hh \text{ (0.60)}$	$\Phi_{+2}^* \rightarrow W^-W^- \text{ (1.0)}$
$\Phi_{+1} \rightarrow t\bar{b} \text{ (0.32)}$	$t\bar{b}hZ \text{ (0.32)}$	$t\bar{b}W^+W^- \text{ (0.10)}$	$t\bar{b}hh \text{ (0.20)}$	—
$\Phi_{+1} \rightarrow hW^+ \text{ (0.68)}$	$hhZW^+ \text{ (0.68)}$	$hW^-W^+W^+ \text{ (0.24)}$	$hhhW^+ \text{ (0.40)}$	—
$A_0 \rightarrow hZ \text{ (1.0)}$	—	$hZW^+W^- \text{ (0.35)}$	$hhhZ \text{ (0.60)}$	—
$H_0 \rightarrow W^+W^- \text{ (0.35)}$	$hZW^+W^- \text{ (0.35)}$	—	—	—
$H_0 \rightarrow hh \text{ (0.60)}$	$hhhZ \text{ (0.60)}$	—	—	—
$\Phi_{+2} \rightarrow W^+W^+ \text{ (1.0)}$	—	—	—	$W^+W^+W^-W^- \text{ (1.0)}$

TABLE I: Final states from Φ production are shown with their branching ratios given in the parentheses at $M_\Phi = 300$ GeV and $v_\Phi = 10^{-2}$ GeV. Only the modes with a branching ratio no less than 0.1 are included.

where L is the integrated luminosity. Given a sufficient number of events N , the mass of a new particle is reconstructed by the invariant mass of combinations of particles in the final state. This procedure can be applied to any signal channels. In Figs. 9 and 10, we present the signal events for each channel versus the new particle masses $M_{\Phi,\Sigma}$ without imposing any cuts. From Fig. 9 one sees that the scalar signal channels are sensitive to v_Φ . In particular, as we discussed earlier, the number of events of $2\ell^\pm 2\ell^\mp$ and $2\ell^\pm 4j$ channels drop rapidly with increasing v_Φ , while the $2\ell^\pm 4j + \cancel{E}_T$ channels behave oppositely. This is understandable since both $2\ell^\pm 2\ell^\mp$ and $2\ell^\pm 4j$ final states include the purely leptonic decay modes of the doubly charged scalars (see Table III), which is significant only for $v_\Phi < 10^{-4}$ GeV. For this reason, we choose two benchmarks in our simulation: $v_\Phi = 10^{-4}$ GeV for the $2\ell^\pm 2\ell^\mp$ and $2\ell^\pm 4j$ channels, and $v_\Phi = 10^{-2}$ GeV for the remaining channels. Finally, we recall that the signal channels of Σ do not depend on v_Φ .

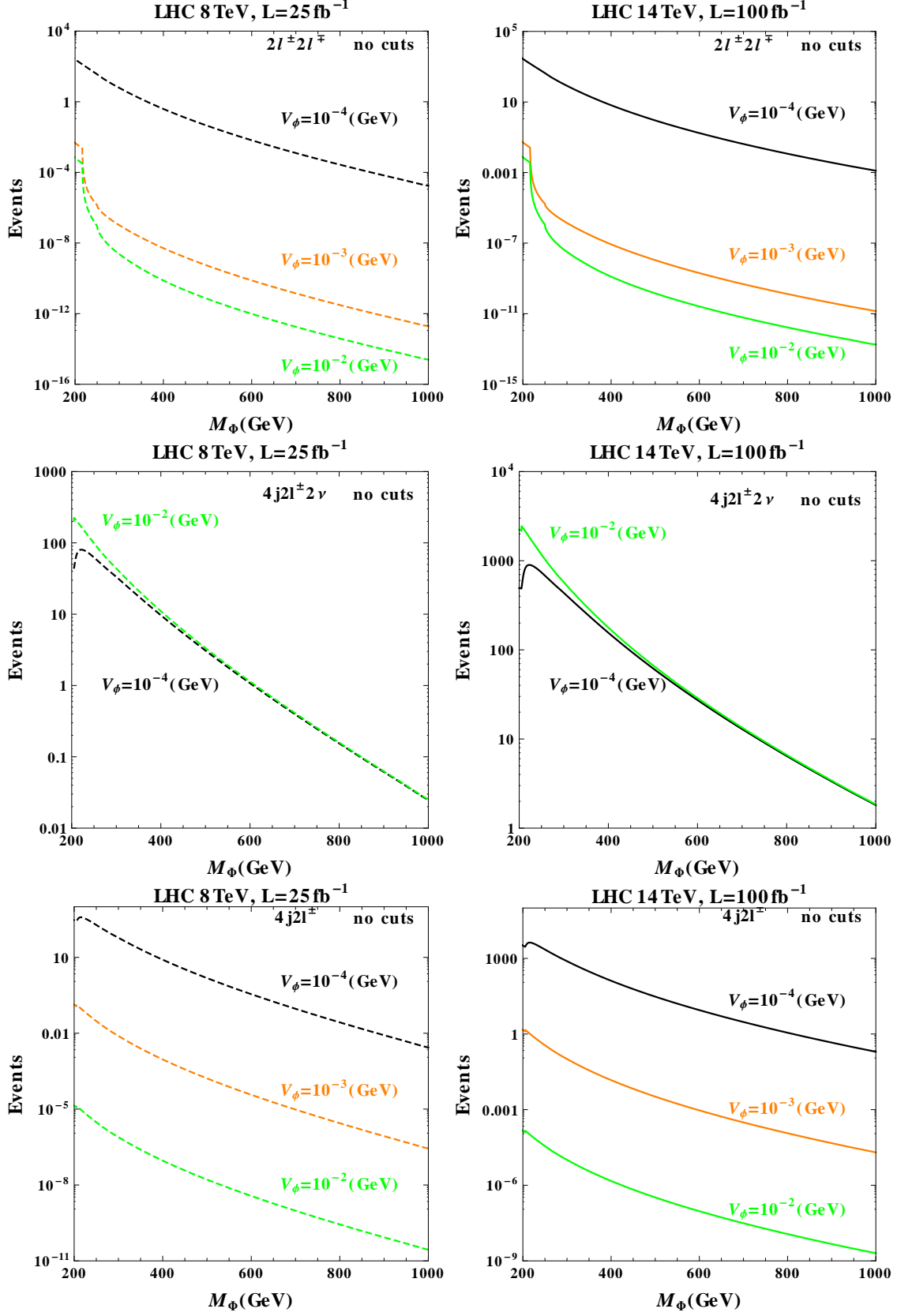


FIG. 9: Predicted number of signals in various channels of Φ production versus M_Φ .

	$\Sigma^+ \rightarrow W^+ \nu$ (0.5)	$\Sigma^+ \rightarrow h\ell^+$ (0.44)	$\Sigma^+ \rightarrow Z\ell^+$ (0.06)	$\Sigma^{++} \rightarrow W^+ \ell^+$ (1.0)
$\Sigma^0 \rightarrow W^\pm \ell^\mp$ (0.5)	$W^\pm W^+ \ell^\mp \nu$ (0.25)	$W^\pm h\ell^\mp \ell^+$ (0.22)	$W^\pm Z\ell^\mp \ell^+$ (0.03)	—
$\Sigma^0 \rightarrow h\nu$ (0.44)	$W^+ h\nu\nu$ (0.22)	$hh\ell^+ \nu$ (0.19)	$Zh\ell^+ \nu$ (0.026)	—
$\Sigma^0 \rightarrow Z\nu$ (0.06)	$W^+ Z\nu\nu$ (0.03)	$Zh\ell^+ \nu$ (0.026)	$ZZ\nu\nu$ (0.0036)	—
$\Sigma^- \rightarrow W^- \nu$ (0.5)	$W^+ W^- \nu\nu$ (0.25)	$hW^- \ell^+ \nu$ (0.22)	$W^- Z\ell^+ \nu$ (0.03)	$W^+ W^- \ell^+ \nu$ (0.5)
$\Sigma^- \rightarrow h\ell^-$ (0.44)	$W^+ h\ell^- \nu$ (0.22)	$hh\ell^+ \ell^-$ (0.19)	$Zh\ell^+ \ell^-$ (0.026)	$W^+ h\ell^+ \ell^-$ (0.44)
$\Sigma^- \rightarrow Z\ell^-$ (0.06)	$W^+ Z\ell^- \nu$ (0.03)	$Zh\ell^+ \ell^-$ (0.026)	$ZZ\ell^+ \ell^-$ (0.0036)	$W^+ Z\ell^+ \ell^-$ (0.06)
$\Sigma^{--} \rightarrow W^- \ell^-$ (1.0)	$W^+ W^- \ell^- \nu$ (0.5)	$W^- h\ell^+ \ell^-$ (0.44)	$W^- Z\ell^+ \ell^-$ (0.06)	$W^+ W^- \ell^+ \ell^-$ (1.0)

TABLE II: Final states from Σ production are shown with their branching ratios given in the parentheses at $M_\Sigma = 300$ GeV and $\nu_\Phi = 10^{-2}$ GeV.

final states	Φ production process in pp collision
$2\ell^\pm 2\ell^\mp$	$\Phi_{+2}\Phi_{+2}^*/A_0H_0 \rightarrow 2\ell^\pm 2\ell^\mp$
$4j2\ell^\pm + \cancel{E_T}$	$\Phi_{+2}\Phi_{+2}^* \rightarrow W^\pm W^\pm W^\mp W^\mp \rightarrow jjjj\ell^\pm \ell^\pm \nu\nu,$ $\Phi_{+2}\Phi_{+1}^*(\Phi_{+2}^*\Phi_{+1}) \rightarrow W^\pm W^\pm + hW^\mp/\bar{t}b(t\bar{b}) \rightarrow jjb\bar{b}\ell^\pm \ell^\pm \nu\nu$
$4j2\ell^\pm$	$\Phi_{+2}\Phi_{+2}^* \rightarrow \ell^\pm \ell^\pm W^\mp W^\mp \rightarrow jjjj\ell^\pm \ell^\pm,$ $\Phi_{+2}\Phi_{+1}^*(\Phi_{+2}^*\Phi_{+1}) \rightarrow \ell^\pm \ell^\pm + hW^\mp/\bar{t}b(t\bar{b}) \rightarrow jjb\bar{b}\ell^\pm \ell^\pm$
final states	Σ production process in pp collision
$2\ell^\pm 2\ell^\mp 2j$	$\Sigma^\pm \Sigma^\mp/\Sigma^0 \Sigma^\pm/\Sigma^\pm \Sigma^\mp \rightarrow hZ(ZZ)\ell^\pm \ell^\mp/W^\pm \ell^\mp Z\ell^\pm/Z\ell^\pm W^\mp \ell^\mp \rightarrow jj2\ell^\pm 2\ell^\mp$
$3\ell^\pm \ell^\mp 2j$	$\Sigma^\pm \Sigma^0 \rightarrow W^\mp \ell^\pm Z\ell^\pm \rightarrow jj3\ell^\pm \ell^\mp$
$3\ell^\pm 2\ell^\mp + \cancel{E_T}$	$\Sigma^\pm \Sigma^0/\Sigma^\pm \Sigma^\mp \rightarrow Z\ell^\pm W^\pm \ell^\mp(Z\ell^\pm Z\nu)/W^\pm \ell^\pm Z\ell^\mp \rightarrow 3\ell^\pm 2\ell^\mp \nu$
$3\ell^\pm 3\ell^\mp$	$\Sigma^\pm \Sigma^\mp \rightarrow \ell^\pm Z\ell^\mp Z \rightarrow 3\ell^\pm 3\ell^\mp$

TABLE III: Signal channels considered and corresponding processes for Φ and Σ production.

The SM backgrounds are also estimated by Madgraph5. For simplicity, we only consider the irreducible backgrounds in our study. We do not include the following backgrounds: (1) multijet final states like the Wnj/Znj production where extra jets come from initial-state or/and final-state radiation and especially pile-up; (2) isolated charged leptons from b quark decays such as the $t\bar{t}/t\bar{t}nj/b\bar{b}nj$ backgrounds; and (3) charged leptons missed by detectors or one jet misidentified as a lepton. Some of them are analyzed and found to be relevant in multi-lepton signal searches

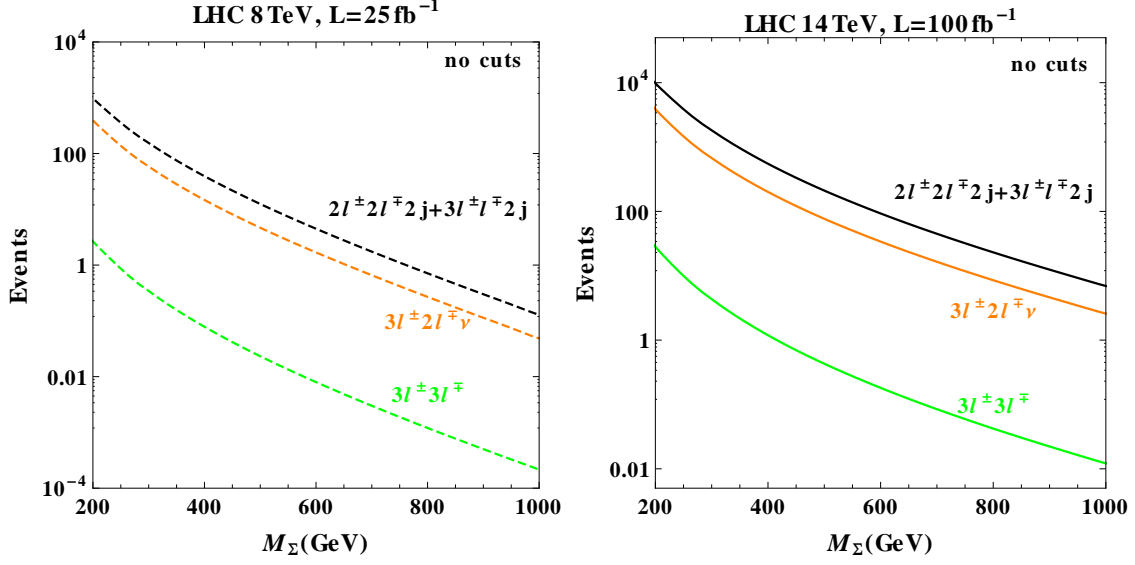


FIG. 10: Predicted number of signals in various channels of Σ production versus M_Σ .

[18]. An accurate prediction of those backgrounds is difficult and can best be estimated from the experimental data which is beyond the scope of our work. Fortunately, for the high p_T leptons which are most relevant to our signals, their effect is estimated to be small.

In the following subsections, we will present our analysis in each signal channel. In signal simulation, we only consider electrons and muons in our definition of a lepton, i.e., $\ell = e, \mu$. For all the channels, we first impose the following basic cuts for the event selection,

$$\begin{aligned}
 p_T(\ell) &> 15 \text{ GeV}, \quad |\eta(\ell)| < 2.5, \\
 p_T(j) &> 20 \text{ GeV}, \quad |\eta(j)| < 2.5, \\
 \Delta R_{\ell\ell} &> 0.4, \quad \Delta R_{j\ell} > 0.4, \quad \Delta R_{jj} > 0.4.
 \end{aligned} \tag{61}$$

After that, specific cut selections are designed according to the properties of final states to reduce the SM background in each channel.

1. Φ production: $4j2\ell^\pm + \cancel{E}_T$ signal

As we discussed above, the pure gauge boson channel becomes dominant for $v_\Phi > 10^{-4}$ GeV, where the doubly charged scalars decay mainly into like-sign di- W 's. Thus the channel $\Phi_{+2} \rightarrow W^+W^+$ serves as the identifier for doubly charged scalars. Although the absence of LNV decays prevents us extracting information on neutrino mass patterns directly, the existence of mixing

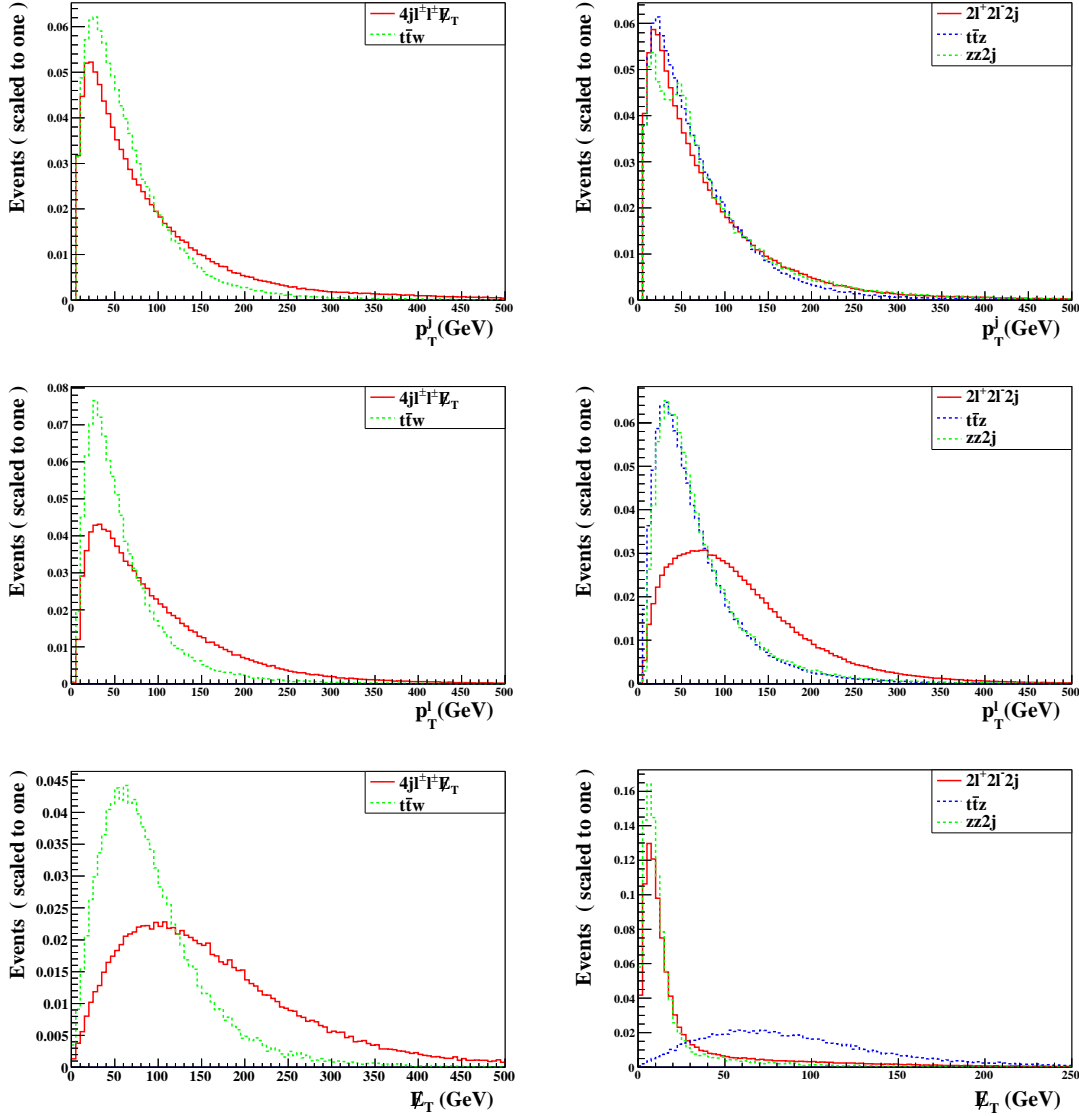


FIG. 11: Distributions of transverse momenta $p_T(\ell)$, $p_T(j)$ and missing energy \cancel{E}_T after imposing basic cuts for the signals $4j2\ell^\pm + \cancel{E}_T$ (left panel) and $2\ell^+2\ell^-2j$ (right) and the backgrounds.

between new scalars and the SM Higgs would indicate that some mechanism of neutrino mass generation is at work. It is helpful to search for channels involving the mixing. These include the following decays whose amplitudes are proportional to v_Φ ,

$$\Phi_{+1} \rightarrow W^+ h / t\bar{b}, \quad H_0 \rightarrow hh, W^+ W^-, \quad A_0 \rightarrow hZ. \quad (62)$$

Both $\Phi_{+1}H_0$ and $\Phi_{+2}\Phi_{+1}^*$ production channels are useful to test gauge couplings and confirm the nature of new scalars. However, it would be difficult to search the channel $H_0\Phi_{+1} \rightarrow hhhW^+$

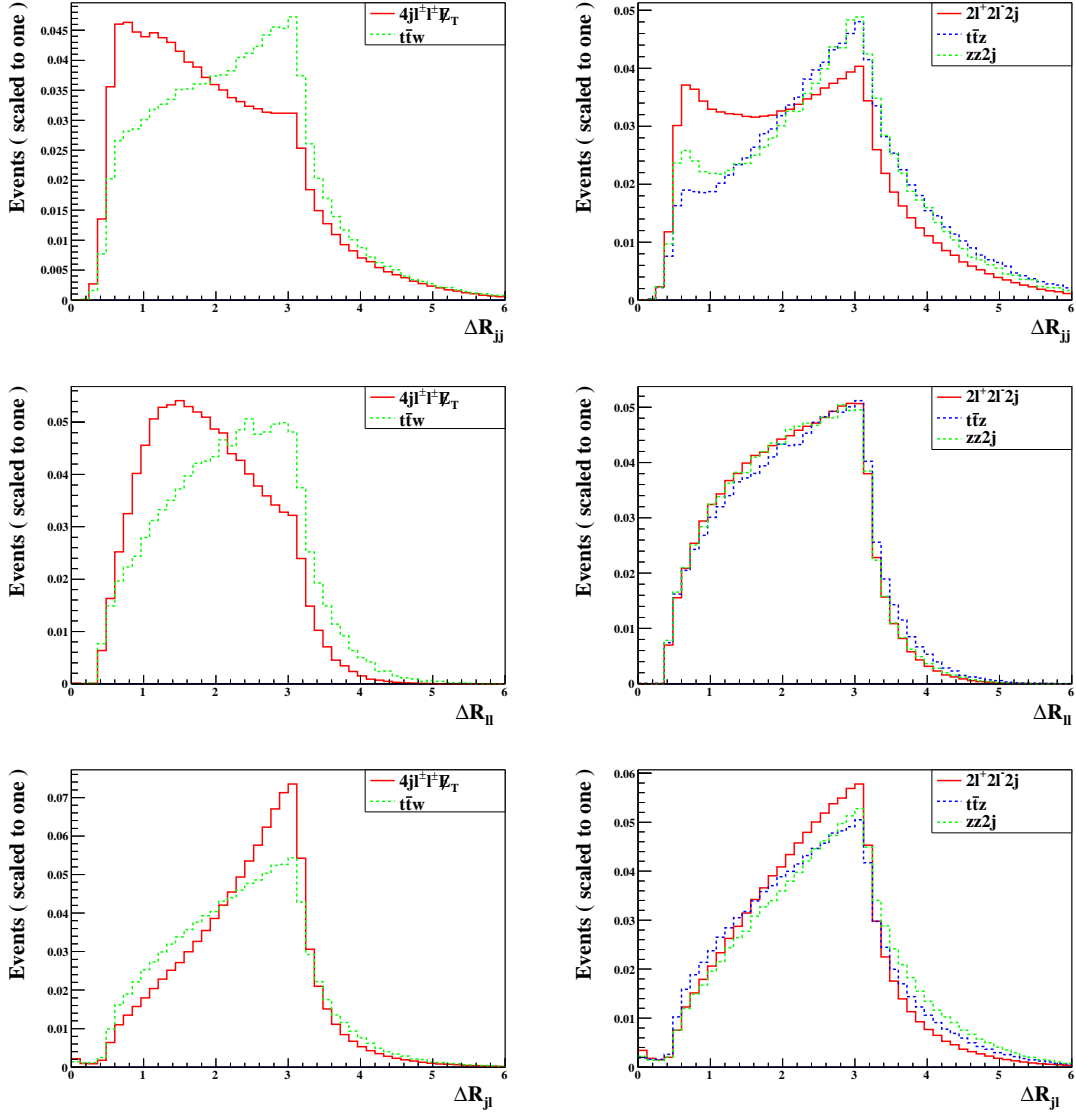


FIG. 12: Similar to Fig. 11, but for distributions of particle separations $\Delta R_{\ell\ell,jj,j\ell}$.

which contains 6 b -jets in the final state. The reconstruction of three SM Higgs bosons from multiple b jets would suffer from large irreducible QCD backgrounds. We thus focus on the $\Phi_{+2}\Phi_{+1}^*/\Phi_{+2}^*\Phi_{+1}$ channels. We reconstruct the events by searching for hadronic decays of like-sign W^\pm pairs from Φ_{+2}/Φ_{+2}^* decays and hadronic decays $W^\mp \rightarrow jj$, $h \rightarrow b\bar{b}$ which in turn come from Φ_{+1}/Φ_{+1}^* decays,

$$pp \rightarrow \Phi_{+2}\Phi_{+1}^*(\Phi_{+2}^*\Phi_{+1}) \rightarrow W^\pm W^\pm + hW^\mp / \bar{t}b(t\bar{b}) \rightarrow jjb\bar{b}\ell^\pm\ell^\pm\nu\nu. \quad (63)$$

The decay branching ratios were given in Fig. 6 and in addition $\text{BR}(h \rightarrow b\bar{b}) \approx 67.7\%$.

The leading irreducible background to this signal is, $t\bar{t}W^\pm \rightarrow jjb\bar{b}W^\pm W^\pm$. Another irreducible background $jjjjW^\pm W^\pm$ is much smaller.² The distributions of transverse momenta $p_T(\ell)$, $p_T(j)$, missing transverse energy \cancel{E}_T and the particle separations $\Delta R_{\ell\ell,jj,j\ell}$ after imposing the basic cuts for both signal and background are displayed in the left panel of Figs. 11 and 12. There are several interesting features for the particle separation distributions. First, the peak of $\Delta R_{j\ell}$ is about 3.0, which indicates that the jets and leptons are isolated enough. Second, the distributions of $\Delta R_{\ell\ell,jj}$ are distinct for signal and background – The leptons and jets from $t\bar{t}W^\pm$ are more isolated than the signal channels. We can thus distinguish between the two by this kinematical variable. To be specific, we apply the following cuts,

$$\Delta R_{jj} < 2.5, \quad \Delta R_{\ell\ell} < 2.5. \quad (64)$$

Additionally, instead of using b tagging, we choose the following cuts on the transverse momentum and missing energy to keep the maximal signal events.

$$p_T(\ell) > 50 \text{ GeV}, \quad p_T(j) > 100 \text{ GeV}, \quad \cancel{E}_T > 30 \text{ GeV}. \quad (65)$$

Since the dijets in the signal come from W or Higgs decays, we require their invariant mass to be in the W/H mass window (with $M_W = 80 \text{ GeV}$ and $M_h = 125 \text{ GeV}$)

$$M_W - 20 \text{ GeV} < M_{jj} < M_h + 25 \text{ GeV}. \quad (66)$$

For the $\Phi_{+2}\Phi_{+1}^*$ channel, one branch of doubly and singly charged scalars gives like-sign dilepton pairs plus large missing energy while the other decays hadronically. We can thus fully reconstruct them through the 4-jet invariant mass M_{jjjj} . At the benchmark point $M_{\Phi_{+2},\Phi_{+1}} = 300 \text{ GeV}$, we require that M_{jjjj} fall into the mass window

$$250 \text{ GeV} < M_{jjjj} < 350 \text{ GeV}. \quad (67)$$

The distribution of M_{jjjj} for both the signal and the leading background $t\bar{t}W^\pm$ are plotted in Fig. 13 at LHC 14 TeV with $L = 100 \text{ fb}^{-1}$. We present in Table IV the survival numbers of events and statistical significance $S/\sqrt{S+B}$ upon imposing the cuts step by step, for LHC 14 TeV and 8 TeV,

² This result is based on the following estimate. Madgraph gives that $jjjW^\pm W^\pm \rightarrow jjj\ell^\pm\ell^\pm\cancel{E}_T$ is about 1.1 (0.31) fb at 14 (8) TeV. We chose the MLM scheme [58] to perform a matching between the soft jets generated by Pythia and the hard jets generated by Madgraph to avoid double counting with a matching scale $x_{\text{qcut}} \sim 60 \text{ GeV}$. Considering additional α_s and phase space suppression, the cross section for $jjjW^\pm W^\pm$ is much smaller than $t\bar{t}W^\pm$.

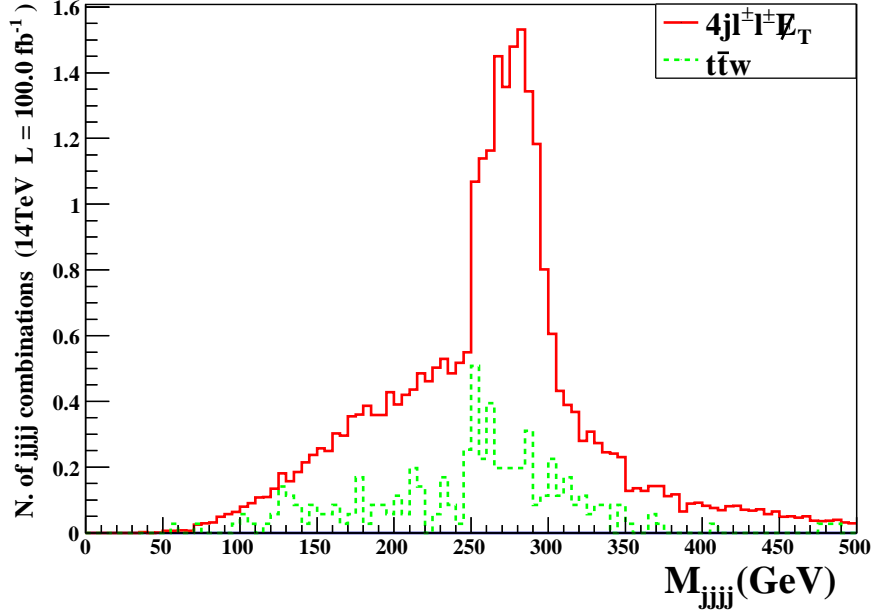


FIG. 13: Reconstruction of doubly and singly charged scalars via 4-jet invariant mass M_{jjjj} for $M_{\Phi_{+2}, \Phi_{+1}} = 300$ GeV at LHC 14 TeV, $L = 100 \text{ fb}^{-1}$. The vertical axis displays the number of four-jet combinations.

respectively. We see that all the cuts chosen here are efficient enough in keeping the signal and suppressing the background. The signal to background ratio can reach 4 : 1 and about 11 signal events survive at LHC 14 TeV. However, the signal is too small to be observable at LHC 8 TeV.

cuts	signal $4j2\ell^\pm + \cancel{E}_T$	bkg $t\bar{t}W^\pm$	$S/\sqrt{S+B}$
no cuts	201 (14.7)	1409 (124)	5.02 (1.25)
basic cuts	143 (11)	851 (82)	4.54 (1.14)
$(\cancel{E}_T, p_T(\ell), p_T(j)) > (30, 50, 100) \text{ GeV}$	118.8 (8.8)	344.4 (30)	5.52 (1.41)
$\Delta R_{jj}, \Delta R_{\ell\ell} < 2.5$	33.04 (2.54)	31.7 (3.05)	4.1 (1.1)
$60 < M_{jj}/\text{GeV} < 150$ ($M_{W,h}$ reconst.)	29.5 (2.3)	28.6 (2.7)	3.87 (1.03)
$250 < M_{jjjj}/\text{GeV} < 350$	11.3 (0.9)	2.5 (0.2)	3.04 (0.85)

TABLE IV: Survival numbers of events and statistical significance $S/\sqrt{S+B}$ after imposing each cut sequentially at $M_{\Phi_{+2}, \Phi_{+1}} = 300$ GeV and for LHC 14 TeV, $L = 100 \text{ fb}^{-1}$ (8 TeV, $L = 25 \text{ fb}^{-1}$ in parentheses).

2. Φ production: $4j2\ell^\pm$ signal

Since the two main decays of Φ_{+2} and Φ_{+2}^* are roughly comparable around $v_\Phi = 10^{-4}$ GeV, we found it advantageous to employ both to select signals in their pair production, with one of them into like-sign dileptons and the other into like-sign di- W 's. In addition, the associated $\Phi_{+2}\Phi_{+1}^*(\Phi_{+2}^*\Phi_{+1})$ production contributes also to the signal. The singly-charged scalar decays to $W^\pm h$ and tb have some features that can be utilized for our purpose. To reduce invisible neutrinos without cutting cross sections too much, we require both the W boson and the SM Higgs decay into hadrons. We apply similar cut selections as in the $4j2\ell^\pm + \cancel{E}_T$ channel except that we do not use cuts on ΔR since the $\Delta R_{\ell\ell,jj}$ distributions for signal and background are not distinct enough, and that the missing energy cut for neutrinos is replaced by a veto cut,

$$\cancel{E}_T < 30 \text{ GeV}. \quad (68)$$

Another difference is that we can now fully reconstruct both doubly and singly charged scalars by forming the 4-jet and dilepton invariant masses. For the former, we adopt the mass window shown in eq. (67), and for the latter, again at the benchmark point $M_{\Phi_{+2},\Phi_{+1}} = 300$ GeV, we assume

$$280 \text{ GeV} < M_{\ell\ell} < 320 \text{ GeV}. \quad (69)$$

Their distributions in the IH and NH cases are displayed in Fig. 14 for LHC 14 TeV, and the number of events is collected in Table V. This channel has considerable signal events and statistical significance, which can reach more than 100 events for the IH case and about 20 events even for the NH with an integrated luminosity of $L = 100 \text{ fb}^{-1}$. The better sensitivity to the IH case is common to both Φ and Σ production signals. It arises as a joint consequence of lepton-flavor dependence in the decay branching ratios of heavy particles, eqs. (58,59) for heavy fermions, and of the fact that only the electrons and muons are counted as leptons in signal simulation. Actually, lepton flavor relations similar to eqs. (58,59) also appear for heavy scalars.

3. Φ production: $2\ell^\pm 2\ell^\mp$ signal

This is a clean channel for the observation of pair production of doubly charged scalars with practically little contamination from the SM background. However, the signal events are also small compared to other channels. Only the $\Phi_{+2}\Phi_{+2}^*$ and $A_0 H_0$ production contributes, and the cross section for the latter is smaller by about an order of magnitude than other channels. Requiring the

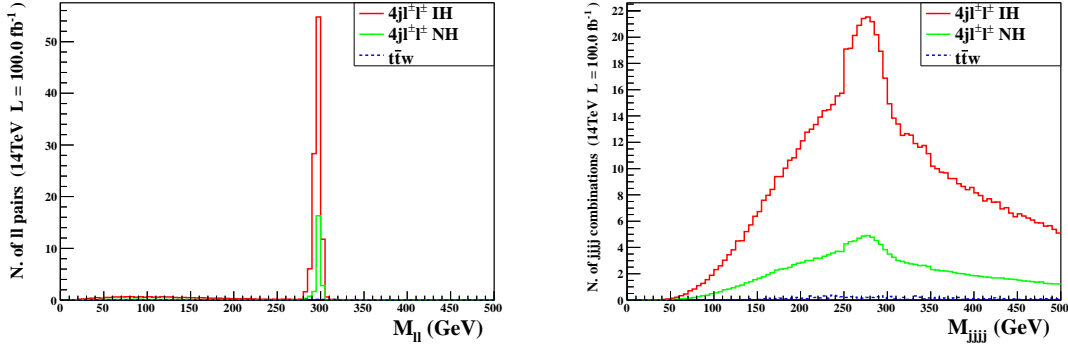


FIG. 14: Reconstruction of doubly and singly charged scalars via the dilepton (left panel) and 4-jet (right) invariant mass for $M_{\Phi_{+2}, \Phi_{+1}} = 300$ GeV at LHC 14 TeV, $L = 100$ fb $^{-1}$.

cuts	signal $4j2\ell^\pm$		bkg $t\bar{t}W^\pm$	$S/\sqrt{S+B}$	
	IH	NH		IH	NH
no cuts	406 (29.7)	81.6 (6)	1409 (124)	9.53 (2.39)	2.11 (0.52)
basic cuts	296.6 (22.5)	60.2 (4.7)	851.3 (81.9)	8.75 (2.2)	1.99 (0.5)
$\cancel{E}_T < 30$ GeV,					
$(p_T(\ell), p_T(j)) > (50, 100)$ GeV	212.4 (16.2)	42.7 (3.4)	36.1 (3.2)	13.47 (3.68)	4.81 (1.31)
$60 < M_{jj}/\text{GeV} < 150$ ($M_{W,h}$ reconst.),					
$280 < M_{ll}/\text{GeV} < 320$	183.1 (13.9)	37.1 (2.9)	1.8 (0.1)	13.47 (3.72)	5.94 (1.67)
$250 < M_{jjjj}/\text{GeV} < 350$	102.6 (7.7)	21.8 (1.7)	0.8 (0.04)	10.09 (2.76)	4.59 (1.27)

TABLE V: Similar to Table IV, but for the $4j2\ell^\pm$ signal and for both NH and IH.

presence of four charged leptons further significantly reduces the signal especially for the NH case, because the charged dilepton decays of $\Phi_{+2}/H_0/A_0$ are highly constrained by the low energy LNV processes. Although there is no intrinsic SM background for the LNV processes, there are some fake ones which can lead to similar final states as our signal. The main irreducible background comes from $ZZ \rightarrow \ell^+\ell^-\ell^+\ell^-$, and the reducible background includes $ZW^+W^- \rightarrow \ell^+\ell^-\ell^+\nu\ell^-\nu$.

For the signal selection, we require the presence of four isolated charged leptons, two positively charged and two negatively charged, whose individual transverse momentum $p_T(\ell)$ must be larger than 50 GeV. The veto cut for the missing transverse energy in eq. (68) is applied to reduce the ZW^+W^- background. And the events containing a pair of oppositely charged leptons with

an invariant mass within 10 GeV around $M_Z \approx 90$ GeV are vetoed. This effectively cuts the ZZ background almost without affecting the signal. Finally, to reconstruct the new scalars, both like-sign dilepton pairs must pass the invariant mass cut in eq. (69).

The invariant mass distribution of the dilepton pairs after all above cuts is displayed in Fig. 15. In Table VI, we collect the event numbers for signal and background upon imposing the cuts step by step. No SM background survives these selections, while only 1.4 (0.11) signal events can be reached for the IH (NH) case. It is worth recalling that the discovery of doubly charged scalars does not require to observe both dilepton pairs with an invariant mass around $M_{\Phi_{+2}}$, but it is sufficient to identify a clear peak in the $M_{\ell\ell}$ distribution [18]. As can be seen in Fig. 15, the peaks are indeed clearly visible for both IH and NH cases, though for NH the number of events at the peak is small even with an integrated luminosity of 100 fb^{-1} .

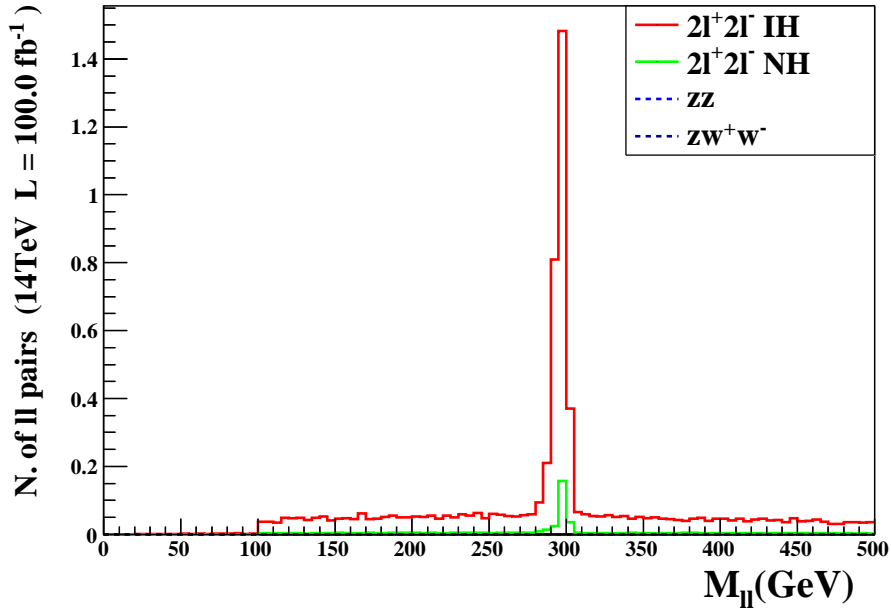


FIG. 15: Reconstruction of doubly charged and neutral scalars via dilepton invariant mass $M_{\ell\ell}$ for $M_{\Phi_{+2}, H_0, A_0} = 300$ GeV at LHC 14 TeV, $L = 100 \text{ fb}^{-1}$.

cuts	signal $2\ell^\pm 2\ell^\mp$		bkg ZZ	bkg ZW^+W^-	$S/\sqrt{S+B}$	
	IH	NH			IH	NH
no cuts	31.6 (2.3)	2.1 (0.15)	4765 (555)	31 (2)	0.45 (0.096)	0.03 (0.0064)
basic cuts	9.7 (0.6)	0.7 (0.04)	610.4 (63.3)	6.4 (0.5)	0.39 (0.07)	0.027 (0.005)
$\cancel{E}_T < 30$ GeV, $p_T^\ell > 50$ GeV	8 (0.5)	0.5 (0.03)	404.2 (43.5)	0.7 (0.06)	0.39 (0.072)	0.026 (0.005)
$80 < M_{\ell^+\ell^-}/\text{GeV} < 100$ (Z veto)	7 (0.4)	0.4 (0.03)	81.3 (8.7)	0.2 (0.02)	0.74 (0.14)	0.05 (0.009)
$280 < M_{\ell^\pm\ell^\pm}/\text{GeV} < 320$	1.4 (0.08)	0.11 (0.006)	0.0 (0.0)	0.0 (0.0)	1.16 (0.28)	0.33 (0.08)

TABLE VI: Similar to Table IV, but for the $2\ell^\pm 2\ell^\mp$ signal and for both IH and NH.

4. Σ production: $2\ell^\pm 2\ell^\mp 2j$ signal

In contrast to the previous LNV four-lepton final states, this signal is common to production of new scalars and fermions. In the latter case, the signal can result from many decay channels of the pair or associated production of fermions,

$$\begin{aligned}
\Sigma^\pm \Sigma^\mp &\rightarrow \ell^\pm Z \ell^\mp Z, \text{ with } ZZ \rightarrow \ell^+ \ell^- q \bar{q}, \\
\Sigma^\pm \Sigma^\mp &\rightarrow \ell^\pm Z \ell^\mp h, \text{ with } Z \rightarrow \ell^+ \ell^-, h \rightarrow q \bar{q}, \\
\Sigma^0 \Sigma^\pm &\rightarrow W^\pm \ell^\mp Z \ell^\pm, \text{ with } Z \rightarrow \ell^+ \ell^-, W \rightarrow q \bar{q}', \\
\Sigma^\pm \Sigma^{\mp\mp} &\rightarrow Z \ell^\pm W^\mp \ell^\mp, \text{ with } Z \rightarrow \ell^+ \ell^-, W \rightarrow q \bar{q}'. \tag{70}
\end{aligned}$$

The main backgrounds are $t\bar{t}Z \rightarrow b\bar{b}\ell^+\ell^-\ell^+\ell^-\nu\nu$ and $ZZ2j \rightarrow \ell^+\ell^-\ell^+\ell^--jj$. Both of them are estimated using Madgraph. For $ZZ2j$, we use the MLM matching scheme assuming $x_{\text{qcut}} = 35$ GeV. The kinematical distributions upon imposing the basic cuts were displayed in the right panel of Figs. 11 and 12. After this, each of the four isolated charged leptons is required to have a transverse momentum no smaller than 50 GeV, and a veto cut $\cancel{E}_T < 30$ GeV facilitates reducing the $t\bar{t}Z$ background. Analogous to the $4j2\ell^\pm + \cancel{E}_T$ final state, the jet separation (see the right panel of Fig. 12) is demanded to be smaller than 2.5 to suppress further the background. Since the signal dijet comes from W, Z, h decays, it helps to separate it from the background by concentrating on the invariant mass window, $60 \text{ GeV} < M_{jj} < 150 \text{ GeV}$. Considering that all channels in eq. (70) involve the decay chain $\Sigma^\pm \rightarrow \ell^\pm Z \rightarrow \ell^\pm \ell^+ \ell^-$, we do not apply Z veto on the dilepton invariant mass $M_{\ell^+\ell^-}$. The heavy mass of Σ^\pm, Σ^0 and $\Sigma^{\mp\mp}$ can be fully reconstructed by forming a triplepton invariant mass $M_{\ell\ell\ell}$ and a dijet-plus-one-lepton invariant mass $M_{jj\ell}$, by focusing on the windows

respectively,

$$280 \text{ GeV} < M_{\ell\ell\ell} < 320 \text{ GeV}, \quad 250 \text{ GeV} < M_{jj\ell} < 350 \text{ GeV}. \quad (71)$$

The resulting distributions are shown in Fig. 16 for both NH and IH cases, and the numbers of events after sequential cuts are collected in Table VII. The final number of signal events can reach 53 (9) at LHC 14 TeV, $L = 100 \text{ fb}^{-1}$ in the IH (NH) case, which looks considerable.

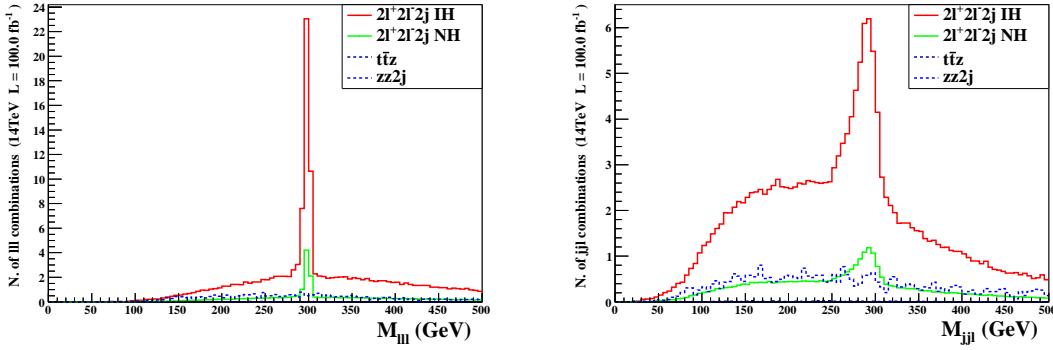


FIG. 16: Reconstruction of Σ^\pm, Σ^0 and $\Sigma^{\mp\mp}$ via a trilepton (left panel) and a dijet-plus-one-lepton (right) invariant mass for $M_{\Sigma^\pm, \Sigma^0} = 300 \text{ GeV}$ at LHC 14 TeV, $L = 100 \text{ fb}^{-1}$.

cuts	signal $2\ell^\pm 2\ell^\mp 2j$		bkg $ZZ2j$	bkg $t\bar{t}Z$	$S/\sqrt{S+B}$	
	IH	NH			IH	NH
no cuts	369 (30)	64.5 (5.3)	402 (34)	198 (10)	11.9 (3.46)	2.5 (0.75)
basic cuts	315.9 (25.8)	55.3 (4.6)	378.8 (32.3)	170.4 (9.3)	10.74 (3.15)	2.25 (0.67)
$\cancel{E}_T < 30 \text{ GeV}, p_T^\ell > 50 \text{ GeV},$						
$\Delta R_{jj} < 2.5$	91.9 (9.1)	15.3 (1.6)	67.6 (6.7)	2.8 (0.2)	7.22 (2.29)	1.66 (0.54)
$60 < M_{jj}/\text{GeV} < 150$ ($M_{W,Z,h}$ reconst.)	74.7 (7.4)	12.3 (1.3)	44 (4.3)	1.7 (0.13)	6.81 (2.15)	1.62 (0.53)
$280 < M_{\ell\ell\ell}/\text{GeV} < 320,$						
$250 < M_{jj\ell}/\text{GeV} < 350$	52.9 (5.3)	9.04 (0.94)	12.5 (1.1)	0.3 (0.016)	6.52 (2.11)	1.94 (0.66)

TABLE VII: Survival numbers of events and statistical significance after imposing each cut sequentially at $M_{\Sigma^\pm, \Sigma^0} = 300 \text{ GeV}$ and for LHC 14 TeV, $L = 100 \text{ fb}^{-1}$ (8 TeV, $L = 25 \text{ fb}^{-1}$).

5. Σ production: $3\ell^\pm\ell^\mp 2j$ signal

The associated production $\Sigma^\pm\Sigma^0$ with decays

$$\Sigma^\pm\Sigma^0 \rightarrow \ell^\pm Z \ell^\pm W^\mp; Z \rightarrow \ell^+\ell^-, W \rightarrow q\bar{q}' \quad (72)$$

can produce a final state containing three leptons of same charge plus one lepton of opposite charge. The irreducible SM background $W^\pm W^\pm Z 2j$ is small enough compared to the signal, thus the basic cuts are sufficient. The Σ^\pm and Σ^0 masses can be reconstructed in a manner similar to that for the preceding $2\ell^\pm 2\ell^\mp 2j$ final state. The resulting two invariant masses $M_{\ell\ell\ell}$ and $M_{jj\ell}$ are plotted in Fig. 17 for $M_{\Sigma^\pm, \Sigma^0} = 300$ GeV. These plots display a clear peak from which M_{Σ^\pm, Σ^0} can be measured. From Table VIII, we see that one can reach statistical significance $S/\sqrt{S+B} \simeq 10$ and expect about 100 signal events in the IH case at LHC 14 TeV, $L = 100 \text{ fb}^{-1}$. It looks also optimistic to discover a signal in this channel for the NH case.

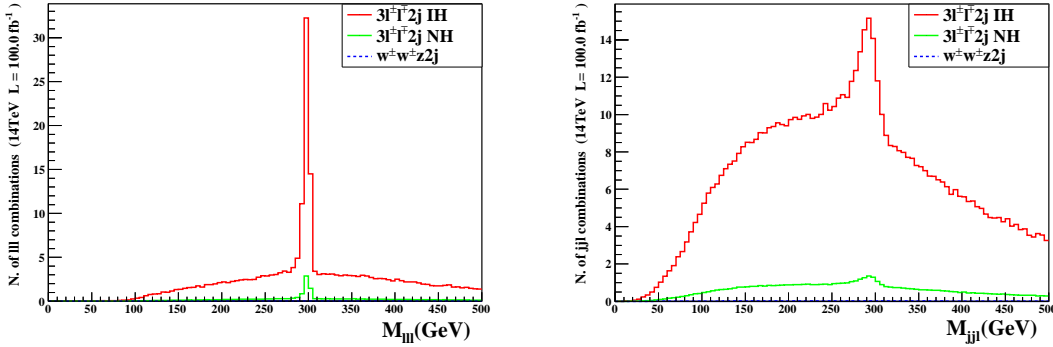


FIG. 17: Reconstruction of Σ^\pm, Σ^0 via a trilepton (left panel) and a dijet-plus-one-lepton (right) invariant mass for $M_{\Sigma^\pm, \Sigma^0} = 300$ GeV at LHC 14 GeV, $L = 100 \text{ fb}^{-1}$.

cuts	signal $3\ell^\pm\ell^\mp 2j$		bkg $W^\pm W^\pm Z 2j$	$S/\sqrt{S+B}$	
	IH	NH		IH	NH
no cuts	121 (9.9)	10.6 (0.8)	0.23 (0.02)	11 (3.15)	3.23 (0.9)
basic cuts	103.3 (8.5)	9.1 (0.7)	0.2 (0.019)	10.15 (2.91)	3 (0.83)

TABLE VIII: Similar to Table VII, but for the $3\ell^\pm\ell^\mp 2j$ signal.

6. Σ production: $3\ell^\pm 2\ell^\mp + \cancel{E}_T$ signal

The five leptons in the final state of this channel can be produced via the decays,

$$\begin{aligned}\Sigma^\pm \Sigma^0 &\rightarrow \ell^\pm Z \ell^\mp W^\pm, \text{ with } Z \rightarrow \ell^+ \ell^-, W \rightarrow \ell \nu, \\ \Sigma^\pm \Sigma^0 &\rightarrow \ell^\pm Z Z \nu, \text{ with both } Z \rightarrow \ell^+ \ell^-, \\ \Sigma^{\pm\pm} \Sigma^\mp &\rightarrow \ell^\pm W^\pm \ell^\mp Z, \text{ with } Z \rightarrow \ell^+ \ell^-, W \rightarrow \ell \nu.\end{aligned}\tag{73}$$

This signal has a much larger branching ratio than the six-lepton signal (see Fig. 10), but still a tiny background, and is thus expected to be more significant. In the event selection, we do not apply any additional criteria beyond the basic cuts. The numbers of events are shown in Table IX. In the IH (NH) scenario, a signal of 50 (15) events is achievable at LHC 14 TeV while it is not quite observable at 8 TeV. Since none of scalar production produces a five-lepton final state, this channel would signal the occurrence of heavy fermion production, albeit only at a relatively large luminosity.

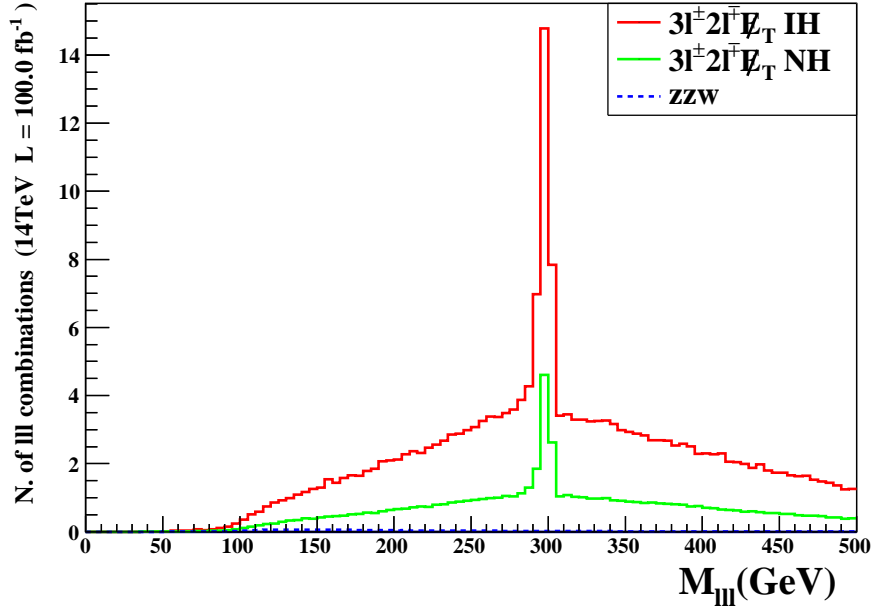


FIG. 18: Reconstruction of Σ^\pm, Σ^0 via a tripleton invariant mass for $M_{\Sigma^\pm} = 300$ GeV at LHC 14 TeV, $L = 100 \text{ fb}^{-1}$.

cuts	signal $3\ell^\pm 2\ell^\mp + \cancel{E}_T$		bkg ZZW^\pm	$S/\sqrt{S+B}$	
	IH	NH		IH	NH
no cuts	157 (12.9)	46.5 (3.8)	3 (0.3)	12.4 (3.55)	6.6 (1.87)
basic cuts	51.2 (3.4)	15 (1)	0.7 (0.06)	7.11 (1.84)	3.78 (0.97)

TABLE IX: Similar to Table VII, but for the $3\ell^\pm 2\ell^\mp + \cancel{E}_T$ signal.

7. Σ production: $3\ell^\pm 3\ell^\mp$ signal

This final channel is the cleanest one but has a tiny cross section. It proceeds exclusively through the following chain,

$$\Sigma^\pm \Sigma^\mp \rightarrow \ell^\pm Z \ell^\mp Z, \text{ with both } Z \rightarrow \ell^+ \ell^-. \quad (74)$$

Upon imposing the basic cuts, we seek six isolated charged leptons, each with a transverse momentum $p_T > 50$ GeV. We further require that both invariant masses $M_{\ell\ell\ell}$ fall in the window $280 - 320$ GeV. The surviving background events after these cuts become practically negligible. However, the signals are also tiny: only 1.6 events are found in the IH scenario and 0.3 events in the NH scenario, even with a very high integrated luminosity of 3000 fb^{-1} . Therefore, this signal channel seems irrelevant for the current and near future LHC run.

cuts	signal $3\ell^\pm 3\ell^\mp$		bkg ZZZ	$S/\sqrt{S+B}$	
	IH	NH		IH	NH
no cuts	13.3 (0.035)	2.4 (0.006)	9.6 (0.031)	2.78 (0.14)	0.68 (0.032)
basic cuts	4.6 (0.01)	0.83 (0.0018)	2.5 (0.007)	1.74 (0.079)	0.45 (0.019)
$p_T^\ell > 50 \text{ GeV}$	4.6 (0.01)	0.82 (0.0018)	2.4 (0.0065)	1.75 (0.08)	0.46 (0.02)
$M_{\ell^+\ell^-} > 90 \text{ GeV}$	4.4 (0.01)	0.8 (0.0017)	2.1 (0.0057)	1.74 (0.08)	0.47 (0.02)
$280 < M_{\ell\ell\ell}/\text{GeV} < 320$	1.6 (0.0038)	0.3 (0.0007)	0.26 (0.0007)	1.15 (0.056)	0.39 (0.019)

TABLE X: Similar to Table VII, but for the $3\ell^\pm 3\ell^\mp$ signal at LHC 14 TeV, $L = 3000 \text{ fb}^{-1}$ (8 TeV, $L = 25 \text{ fb}^{-1}$ in parentheses).

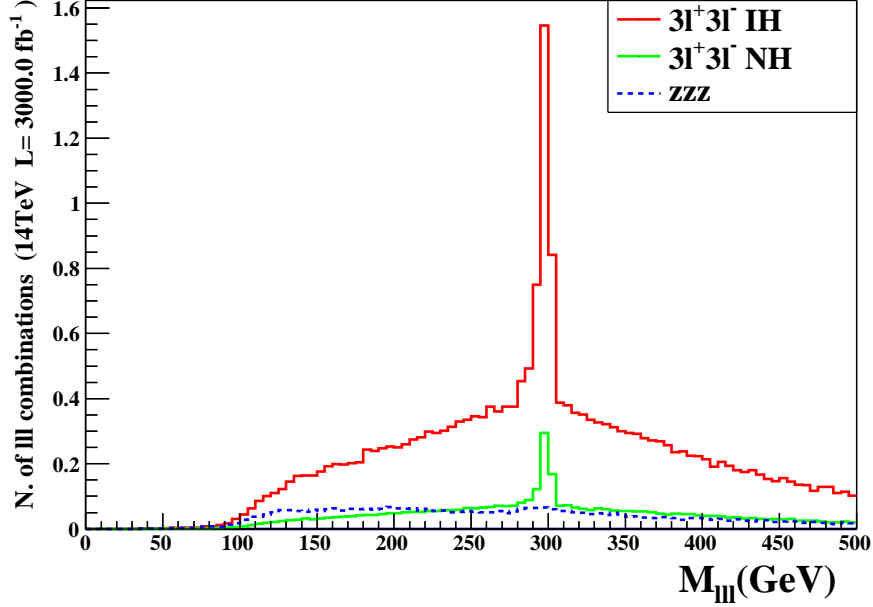


FIG. 19: Reconstruction of Σ^\pm via trilepton invariant mass for $M_{\Sigma^\pm} = 300$ GeV at LHC 14 TeV, $L = 3000 \text{ fb}^{-1}$.

V. CONCLUSIONS

We have carried out a careful study of the minimal version of the cascade seesaw [44] in both theoretical and phenomenological aspects. We have made a comprehensive analysis on low-energy LFV constraints and LHC signatures. For this, we have developed a UFO model by means of FeynRules package, which can also be applied to phenomenological studies for other seesaw mechanisms.

The main features and results are as follows:

- We introduced a convenient framework to handle Yukawa couplings. Based on a parametrization trick in Ref. [45], all mixing matrices are expressed in terms of the quadruplet scalar VEV v_Φ , a complex parameter t and known neutrino parameters. Together with heavy particle masses this fixes all production rates and decay branching ratios of heavy particles. This facilitates our phenomenological analysis significantly.
- We considered systematically the contributions of new interactions to the stringently constrained LFV transitions, including the decays $\mu \rightarrow e\gamma, 3e$ and μ - e conversion in nuclei. We

found that the strictest constraint comes from the upper bound on the decay $\mu \rightarrow e\gamma$. For instance, for heavy masses of 200 – 300 GeV, the scalar VEV v_Φ must be at least of order 10^{-4} GeV. This significantly affects the decays of heavy particles. Inclusion of low-energy constraints makes our collider study realistic.

- We examined all relevant decays of new particles at some benchmark points of free parameters, keeping an eye on their impact on the detection strategy at LHC. We explored LHC signatures by surveying potentially interesting signal channels. For the detection of quadruplet scalars, the $4j2\ell^\pm$ signal is most important, and it has significant signal events and statistical significance. And for the quintuplet fermions, the $2\ell^\pm 2\ell^\mp 2j$, $3\ell^\pm \ell^\mp 2j$ and $3\ell^\pm 2\ell^\mp + E_T$ signals are quite promising.

Notes added

During the finishing stage of this work, a new preprint [59] appeared that also studied the LHC signatures of the model. Here we discuss briefly some of the differences between that work and ours. (1) The authors in [59] did not consider the mixing of quadruplet scalars and quintuplet fermions, so that their decay modes of the new particles are much less than ours. For instance, they claimed that the Φ_{+2} coupling to dileptons is absent, thus Φ_{+2} decays always dominantly into di- W 's. Our study indicates that the two decay modes are actually comparable around $v_\Phi \sim 10^{-4}$ GeV. (2) They treated the Yukawa couplings and the VEV v_Φ as free parameters. Our analysis tells that the two are correlated by constraints from low-energy LFV transitions. These two differences affect the LHC analysis in a significant manner. (3) The choice of signal channels and the corresponding cut selections are distinct between the two papers.

Acknowledgement

RD would like to thank Kai Wang for useful discussion at the beginning of this work and Liang-Liang Zhang for help on data analysis. This work was supported in part by the grants NSFC-11025525 and NSFC-11205113.

APPENDIX A: Some details on the minimal cascade seesaw model

We first list the gauge interactions of the Φ field. Together with the usual interactions of the SM ϕ field and upon incorporating their mixing, one obtains the gauge couplings of the physical scalars and the would-be Goldstone bosons.

The trilinear terms linear in v_Φ are

$$\begin{aligned} \mathcal{L} \supset & g_2^2 v_\Phi \left[\left(\sqrt{3}(W_\mu^+)^2 \Phi_{+2}^* + \text{h.c.} \right) + \frac{7}{\sqrt{2}} W_\mu^+ W^{\mu-} \text{Re} \Phi_0 + \frac{1}{2\sqrt{2}c_W^2} Z_\mu Z^\mu \text{Re} \Phi_0 \right. \\ & \left. + c_W^{-1} Z^\mu \left(\frac{1}{2} \sqrt{6}(1+s_W^2) W_\mu^+ \Phi_{-1} - 2s_W^2 W_\mu^+ \Phi_{+1}^* + \text{h.c.} \right) \right] \\ & + \frac{1}{\sqrt{2}} e g_2 v_\Phi A^\mu \left[W_\mu^+ (2\Phi_{+1}^* - \sqrt{3}\Phi_{-1}) + \text{h.c.} \right], \end{aligned} \quad (75)$$

while the other trilinear terms are

$$\begin{aligned} \mathcal{L} \supset & \frac{ig_2}{\sqrt{2}} W^{\mu+} \left[\sqrt{3}(\Phi_0^* \partial_\mu \Phi_{-1} - \Phi_{-1} \partial_\mu \Phi_0^*) + 2(\Phi_{+1}^* \partial_\mu \Phi_0 - \Phi_0 \partial_\mu \Phi_{+1}^*) \right. \\ & \left. + \sqrt{3}(\Phi_{+2}^* \partial_\mu \Phi_{+1} - \Phi_{+1} \partial_\mu \Phi_{+2}^*) \right] + \text{h.c.} \\ & + \frac{ig_2}{2c_W} Z^\mu \left[(3-4s_W^2) \Phi_{+2}^* \partial_\mu \Phi_{+2} + (1-2s_W^2) \Phi_{+1}^* \partial_\mu \Phi_{+1} \right. \\ & \left. - \Phi_0^* \partial_\mu \Phi_0 + (-3+2s_W^2) \Phi_{-1}^* \partial_\mu \Phi_{-1} \right] \\ & + ie A^\mu \left[2\Phi_{+2}^* \partial_\mu \Phi_{+2} + \Phi_{+1}^* \partial_\mu \Phi_{+1} - \Phi_{-1}^* \partial_\mu \Phi_{-1} \right]. \end{aligned} \quad (76)$$

The quartic gauge interaction terms of Φ are

$$\begin{aligned} \mathcal{L} \supset & +\sqrt{3}g_2^2 \left[W_\mu^+ W^{+\mu} (\Phi_{-1} \Phi_{+1}^* + \Phi_0 \Phi_{+2}^*) + \text{h.c.} \right] \\ & + \frac{1}{2} g_2^2 W_\mu^+ W^{-\mu} (3|\Phi_{+2}|^2 + 7|\Phi_{+1}|^2 + 7|\Phi_0|^2 + 3|\Phi_{-1}|^2) \\ & + \frac{g_2^2}{\sqrt{2}c_W} Z^\mu \left[W_\mu^+ \left(\sqrt{3}(2-3s_W^2) \Phi_{+1} \Phi_{+2}^* - 2s_W^2 \Phi_0 \Phi_{+1}^* + \sqrt{3}(-2+s_W^2) \Phi_{-1} \Phi_0^* \right) + \text{h.c.} \right] \\ & + \frac{eg_2}{\sqrt{2}} A^\mu \left[W_\mu^+ \left(3\sqrt{3} \Phi_{+1} \Phi_{+2}^* + 2\Phi_0 \Phi_{+1}^* - \sqrt{3} \Phi_{-1} \Phi_0^* \right) + \text{h.c.} \right] \\ & + \frac{g_2^2}{4c_W^2} Z_\mu Z^\mu \left[(3-4s_W^2)^2 |\Phi_{+2}|^2 + (1-2s_W^2)^2 |\Phi_{+1}|^2 + |\Phi_0|^2 + (3-2s_W^2)^2 |\Phi_{-1}|^2 \right] \\ & + \frac{eg_2}{c_W} Z_\mu A^\mu \left[2(3-4s_W^2) |\Phi_{+2}|^2 + (1-2s_W^2) |\Phi_{+1}|^2 - (3+2s_W^2) |\Phi_{-1}|^2 \right] \\ & + e^2 A_\mu A^\mu \left[4|\Phi_{+2}|^2 + |\Phi_{+1}|^2 + |\Phi_{-1}|^2 \right]. \end{aligned} \quad (77)$$

The explicit forms of the mixing coupling matrices appearing in eq. (33) are,

$$\begin{aligned}
\mathcal{W}_L &= U_N^\dagger w_L U_L = \begin{pmatrix} U_{\text{PMNS}}^\dagger \left(\mathbf{1}_3 + \frac{7}{4M_\Sigma} ZZ^\dagger \right) & -\sqrt{\frac{3}{2}} U_{\text{PMNS}}^\dagger Z / \sqrt{M_\Sigma} \\ -2Z^\dagger / \sqrt{M_\Sigma} & \sqrt{6} \mathbf{1}_2 \end{pmatrix}, \\
\mathcal{W}_R &= U_N^T w_R U_R = \begin{pmatrix} 0_3 & -\sqrt{6} U_{\text{PMNS}}^T Z^* / \sqrt{M_\Sigma} \\ -3\eta^\dagger & \sqrt{6} \mathbf{1}_2 \end{pmatrix}, \\
\mathcal{W}_L^D &= U_L^\dagger w_D = \begin{pmatrix} -\sqrt{\frac{3}{2M_\Sigma}} Z \\ \mathbf{1}_2 \end{pmatrix}, \quad \mathcal{W}_R^D = U_R^\dagger w_D = \begin{pmatrix} -\sqrt{\frac{3}{2}} \eta \\ \mathbf{1}_2 \end{pmatrix}, \\
\mathcal{Z}_L^v &= U_N^\dagger z_L^N U_N = \frac{1}{2} \begin{pmatrix} \mathbf{1}_3 - U_{\text{PMNS}}^\dagger ZZ^\dagger U_{\text{PMNS}} / M_\Sigma & U_{\text{PMNS}}^\dagger Z / \sqrt{M_\Sigma} \\ Z^\dagger U_{\text{PMNS}} / \sqrt{M_\Sigma} & Z^\dagger Z / M_\Sigma \end{pmatrix}, \\
\mathcal{Z}_L^\ell &= U_L^\dagger z_L^E U_L = \left(-\frac{1}{2} + s_W^2 \right) \mathbf{1}_5 - \frac{1}{2} \begin{pmatrix} \frac{3}{2M_\Sigma} ZZ^\dagger & -\sqrt{\frac{3}{2M_\Sigma}} Z \\ -\sqrt{\frac{3}{2M_\Sigma}} Z^\dagger & \mathbf{1}_2 \end{pmatrix}, \\
\mathcal{Z}_R^\ell &= U_R^\dagger z_R^E U_R = s_W^2 \mathbf{1}_5 - \begin{pmatrix} \frac{3}{2} \eta \eta^\dagger & -\sqrt{\frac{3}{2}} \eta \\ -\sqrt{\frac{3}{2}} \eta^\dagger & \mathbf{1}_2 \end{pmatrix}.
\end{aligned} \tag{78}$$

APPENDIX B: Loop functions

The functions appearing in the radiative transitions are

$$\begin{aligned}
F^a(r) &= \frac{1}{12(1-r)^4} [1 - 6r + 3r^2 + 2r^3 - 6r^2 \ln r], \\
F^b(r) &= -\frac{1}{12(1-r)^4} [2 + 3r - 6r^2 + r^3 + 6r \ln r], \\
G^a(r) &= \frac{1}{36(1-r)^4} [2 - 9r + 18r^2 - 11r^3 + 6r^3 \ln r], \\
G^b(r) &= \frac{1}{36(1-r)^4} [-16 + 45r - 36r^2 + 7r^3 - 12 \ln r + 18r \ln r],
\end{aligned} \tag{79}$$

and the function from the box diagram in Fig. 2 is

$$H(r) = \frac{1}{4(1-r)^3} r(1 - r^2 + 2r \ln r). \tag{80}$$

APPENDIX C: Decay widths of heavy particles

Listed below are the approximate expressions for the relevant decay widths in the degenerate case studied in this work.

Doubly charged scalar Φ_{+2} :

$$\Gamma(\Phi_{+2} \rightarrow \ell_i^+ \ell_j^+) = \frac{3M_\Phi |(ZZ^\dagger)_{ij}|^2}{16\pi v_\Phi^2 (1 + \delta_{ij})}, \quad (81)$$

$$\Gamma(\Phi_{+2} \rightarrow W^+ W^+) = \frac{3v_\Phi^2 M_\Phi^3}{2\pi v_\phi^4} \left(1 - 4\frac{M_W^2}{M_\Phi^2}\right)^{\frac{1}{2}} \left(1 - 4\frac{M_W^2}{M_\Phi^2} + 12\frac{M_W^4}{M_\Phi^4}\right). \quad (82)$$

Singly charged scalar Φ_{+1} :

$$\Gamma(\Phi_{+1} \rightarrow t\bar{b}) = \frac{3M_t^2 v_\Phi^2 M_\Phi}{\pi v_\phi^4} \left(1 - \frac{M_t^2}{M_\Phi^2}\right)^2, \quad (83)$$

$$\Gamma(\Phi_{+1} \rightarrow \ell_i^+ \nu_j) = \frac{M_\Phi |(ZZ^\dagger)_{ij}|^2}{64\pi v_\Phi^2}, \quad (84)$$

$$\Gamma(\Phi_{+1} \rightarrow hW^+) = \frac{2v_\Phi^2 M_\Phi^3}{\pi v_\phi^4} \left[\frac{M_h^4}{M_\Phi^4} + \left(1 - \frac{M_W^2}{M_\Phi^2}\right)^2 - 2\frac{M_h^2}{M_\Phi^2} \left(1 + \frac{M_W^2}{M_\Phi^2}\right)^2 \right]^{\frac{3}{2}}. \quad (85)$$

CP-even neutral scalar H_0 :

$$\Gamma(H_0 \rightarrow b\bar{b}) = \frac{27M_b^2 v_\Phi^2 M_\Phi}{4\pi v_\phi^4}, \quad (86)$$

$$\Gamma(H_0 \rightarrow t\bar{t}) = \frac{27M_t^2 v_\Phi^2 M_\Phi}{4\pi v_\phi^4} \left(1 - \frac{M_t^2}{M_\Phi^2}\right)^2, \quad (87)$$

$$\Gamma(H_0 \rightarrow \ell_i^+ \ell_j^-) = \frac{9M_\Phi |(ZZ^\dagger)_{ij}|^2}{32\pi v_\Phi^2 (1 + \delta_{ij})}, \quad (88)$$

$$\Gamma(H_0 \rightarrow \nu_i \nu_j) = \frac{M_\Phi |(ZZ^\dagger)_{ij}|^2}{4\pi v_\Phi^2 (1 + \delta_{ij})}, \quad (89)$$

$$\Gamma(H_0 \rightarrow hh) \approx \frac{7v_\Phi^2 M_\Phi^3}{2\pi v_\phi^4} \left(1 - 4\frac{M_h^2}{M_\Phi^2}\right)^{\frac{1}{2}}, \quad (90)$$

$$\Gamma(H_0 \rightarrow W^+ W^-) = \frac{2v_\Phi^2 M_\Phi^3}{\pi v_\phi^4} \left(1 - 4\frac{M_W^2}{M_\Phi^2}\right)^{\frac{1}{2}} \left(1 - 4\frac{M_W^2}{M_\Phi^2} + 12\frac{M_W^4}{M_\Phi^4}\right), \quad (91)$$

$$\Gamma(H_0 \rightarrow ZZ) = \frac{v_\Phi^2 M_\Phi^3}{4\pi v_\phi^4} \left(1 - 4\frac{M_Z^2}{M_\Phi^2}\right)^{\frac{1}{2}} \left(1 - 4\frac{M_Z^2}{M_\Phi^2} + 12\frac{M_Z^4}{M_\Phi^4}\right). \quad (92)$$

CP-odd neutral scalar A_0 :

$$\Gamma(A_0 \rightarrow b\bar{b}) = \frac{3M_b^2 v_\Phi^2 M_\Phi}{4\pi v_\phi^4}, \quad (93)$$

$$\Gamma(A_0 \rightarrow t\bar{t}) = \frac{3M_t^2 v_\Phi^2 M_\Phi}{4\pi v_\phi^4} \left(1 - \frac{M_t^2}{M_\Phi^2}\right)^2, \quad (94)$$

$$\Gamma(A_0 \rightarrow \ell_i^+ \ell_j^-) = \frac{9M_\Phi |(ZZ^\dagger)_{ij}|^2}{32\pi v_\Phi^2 (1 + \delta_{ij})}, \quad (95)$$

$$\Gamma(A_0 \rightarrow \nu_i \nu_j) = \frac{M_\Phi |(ZZ^\dagger)_{ij}|^2}{4\pi v_\Phi^2 (1 + \delta_{ij})}, \quad (96)$$

$$\Gamma(A_0 \rightarrow hZ) = \frac{2v_\Phi^2 M_\Phi^3}{\pi v_\phi^4} \left[1 + \left(\frac{M_h^2}{M_\Phi^2} - \frac{M_Z^2}{M_\Phi^2} \right)^2 - 2 \left(\frac{M_h^2}{M_\Phi^2} - \frac{M_Z^2}{M_\Phi^2} \right) \right]^{\frac{3}{2}}. \quad (97)$$

Singly charged scalar Φ_{-1} :

$$\Gamma(\Phi_{-1} \rightarrow \bar{t}b) = \frac{9M_t^2 v_\Phi^2 M_\Phi}{4\pi v_\phi^4} \left(1 - \frac{M_t^2}{M_\Phi^2}\right)^2, \quad (98)$$

$$\Gamma(\Phi_{-1} \rightarrow \ell_i^- \nu_j) = \frac{3M_\Phi |(ZZ^\dagger)_{ij}|^2}{64\pi v_\Phi^2}, \quad (99)$$

$$\Gamma(\Phi_{-1} \rightarrow hW^-) = \frac{3v_\Phi^2 M_\Phi^3}{4\pi v_\phi^4} \left[\frac{M_h^4}{M_\Phi^4} + \left(1 - \frac{M_W^2}{M_\Phi^2}\right)^2 - 2 \frac{M_h^2}{M_\Phi^2} \left(1 + \frac{M_W^2}{M_\Phi^2}\right)^2 \right]^{\frac{3}{2}}, \quad (100)$$

$$\begin{aligned} \Gamma(\Phi_{-1} \rightarrow ZW^-) &= \frac{3v_\Phi^2 M_\Phi^3}{2\pi v_\phi^4} \left[1 + \left(\frac{M_W^2}{M_\Phi^2} - \frac{M_Z^2}{M_\Phi^2} \right)^2 - 2 \left(\frac{M_W^2}{M_\Phi^2} + \frac{M_Z^2}{M_\Phi^2} \right) \right]^{1/2}, \\ &\times \left[1 + \frac{M_W^4}{M_\Phi^4} + 10 \frac{M_W^2}{M_\Phi^2} \frac{M_Z^2}{M_\Phi^2} + \frac{M_Z^4}{M_\Phi^4} - 2 \left(\frac{M_W^2}{M_\Phi^2} + \frac{M_Z^2}{M_\Phi^2} \right) \right]. \end{aligned} \quad (101)$$

Neutral heavy fermion Σ^0 :

$$\Gamma(\Sigma_i^0 \rightarrow W^\pm \ell_j^\mp) = \frac{g_2^2}{64\pi} 4|Z_{ji}|^2 \frac{M_\Sigma^2}{M_W^2} \left(1 - \frac{M_W^2}{M_\Sigma^2}\right) \left(1 + \frac{M_W^2}{M_\Sigma^2} - 2 \frac{M_W^4}{M_\Sigma^4}\right), \quad (102)$$

$$\sum_{l=e}^{\tau} \Gamma(\Sigma_i^0 \rightarrow Z\nu_l) = \frac{g_2^2}{64\pi c_W^2} \sum_{l=e}^{\tau} |Z_{li}|^2 \frac{M_\Sigma^2}{M_Z^2} \left(1 - \frac{M_Z^2}{M_\Sigma^2}\right)^2 \left(1 + 2 \frac{M_Z^2}{M_\Sigma^2}\right), \quad (103)$$

$$\sum_{l=e}^{\tau} \Gamma(\Sigma_i^0 \rightarrow h\nu_l) \approx \frac{g_2^2}{64\pi} 9 \sum_{l=e}^{\tau} |Z_{li}|^2 \frac{M_\Sigma^2}{M_W^2} \left(1 - \frac{M_h^2}{M_\Sigma^2}\right)^2. \quad (104)$$

Singly charged heavy fermion Σ^- :

$$\sum_{l=e}^{\tau} \Gamma(\Sigma_i^- \rightarrow W^- \nu_l) = \frac{g_2^2}{64\pi} \sum_{l=e}^{\tau} \frac{15}{2} |Z_{li}|^2 \frac{M_{\Sigma}^2}{M_W^2} \left(1 - \frac{M_W^2}{M_{\Sigma}^2}\right)^2 \left(1 + 2 \frac{M_W^2}{M_{\Sigma}^2}\right), \quad (105)$$

$$\Gamma(\Sigma_i^- \rightarrow Z \ell_j^-) = \frac{g_2^2}{64\pi c_W^2} \frac{3}{4} |Z_{ji}|^2 \frac{M_{\Sigma}^2}{M_Z^2} \left(1 - \frac{M_Z^2}{M_{\Sigma}^2}\right) \left(1 + \frac{M_Z^2}{M_{\Sigma}^2} - 2 \frac{M_Z^4}{M_{\Sigma}^4}\right), \quad (106)$$

$$\Gamma(\Sigma_i^- \rightarrow h \ell_j^-) \approx \frac{g_2^2}{64\pi} \frac{27}{4} |Z_{li}|^2 \frac{M_{\Sigma}^2}{M_W^2} \left(1 - \frac{M_h^2}{M_{\Sigma}^2}\right)^2. \quad (107)$$

Doubly charged heavy fermion Σ^{--} :

$$\Gamma(\Sigma_i^{--} \rightarrow W^- \ell_j^-) = \frac{g_2^2}{64\pi} 6 |Z_{ji}|^2 \frac{M_{\Sigma}^3}{M_W^2} \left(1 - \frac{M_W^2}{M_{\Sigma}^2}\right) \left(1 + \frac{M_W^2}{M_{\Sigma}^2} - 2 \frac{M_W^4}{M_{\Sigma}^4}\right). \quad (108)$$

-
- [1] S. Weinberg, Phys. Rev. Lett. **43**, 1566 (1979).
 - [2] E. Ma, Phys. Rev. Lett. **81**, 1171 (1998) [arXiv:hep-ph/9805219].
 - [3] M. Gell-Mann, P. Ramond, R. Slansky, in: D. Freedman, P. van Nieuwenhuizen (Eds.), Supergravity, North-Holland, Amsterdam, 1979, p.315; T. Yanagida, in: O. Sawada, A. Sugamoto (Eds.), Proceedings of the Workshop on Unified Theory and Baryon Number in the Universe, KEK, Japan, 1979; R.N. Mohapatra, G. Senjanovic, Phys. Rev. Lett. **44** (1980) 912.
 - [4] W. Konetschny and W. Kummer, Phys. Lett. B **70**, 433 (1977); T. P. Cheng and L. F. Li, Phys. Rev. D **22**, 2860 (1980); J. Schechter and J. W. F. Valle, Phys. Rev. D **22**, 2227 (1980); R. N. Mohapatra and G. Senjanovic, Phys. Rev. D **23**, 165 (1981); G. Lazarides, Q. Shafi and C. Wetterich, Nucl. Phys. B **181**, 287 (1981).
 - [5] R. Foot, H. Lew, X. G. He and G. C. Joshi, Z. Phys. C **44**, 441 (1989).
 - [6] T. Han and B. Zhang, Phys. Rev. Lett. **97**, 171804 (2006) [hep-ph/0604064].
 - [7] A. Atre, T. Han, S. Pascoli and B. Zhang, JHEP **0905**, 030 (2009) [arXiv:0901.3589 [hep-ph]].
 - [8] F. del Aguila, J. A. Aguilar-Saavedra and R. Pittau, JHEP **0710**, 047 (2007) [hep-ph/0703261].
 - [9] J. Kersten and A. Y. Smirnov, Phys. Rev. D **76** (2007) 073005 [arXiv:0705.3221 [hep-ph]].
 - [10] P. S. B. Dev, A. Pilaftsis and U. -k. Yang, Phys. Rev. Lett. **112**, 081801 (2014) [arXiv:1308.2209 [hep-ph]].
 - [11] T. Han, B. Mukhopadhyaya, Z. Si and K. Wang, Phys. Rev. D **76**, 075013 (2007) [arXiv:0706.0441 [hep-ph]].

- [12] P. Fileviez Perez, T. Han, G. -y. Huang, T. Li and K. Wang, Phys. Rev. D **78**, 015018 (2008) [arXiv:0805.3536 [hep-ph]].
- [13] J. Garayoa and T. Schwetz, JHEP **0803**, 009 (2008) [arXiv:0712.1453 [hep-ph]].
- [14] A. G. Akeroyd, M. Aoki and H. Sugiyama, Phys. Rev. D **77**, 075010 (2008) [arXiv:0712.4019 [hep-ph]].
- [15] R. Franceschini, T. Hambye and A. Strumia, Phys. Rev. D **78** (2008) 033002 [arXiv:0805.1613 [hep-ph]].
- [16] T. Li and X. -G. He, Phys. Rev. D **80**, 093003 (2009) [arXiv:0907.4193 [hep-ph]].
- [17] C. Biggio and F. Bonnet, Eur. Phys. J. C **72** (2012) 1899 [arXiv:1107.3463 [hep-ph]].
- [18] F. del Aguila and J. A. Aguilar-Saavedra, Nucl. Phys. B **813**, 22 (2009) [arXiv:0808.2468 [hep-ph]].
- [19] S. Chatrchyan *et al.* [CMS Collaboration], Eur. Phys. J. C **72**, 2189 (2012) [arXiv:1207.2666 [hep-ex]].
- [20] S. Chatrchyan *et al.* [CMS Collaboration], Phys. Lett. B **717**, 109 (2012) [arXiv:1207.6079 [hep-ex]].
- [21] [ATLAS Collaboration], ATLAS-CONF-2012-139.
- [22] G. Aad *et al.* [ATLAS Collaboration], Eur. Phys. J. C **72**, 2244 (2012) [arXiv:1210.5070 [hep-ex]].
- [23] S. Chatrchyan *et al.* [CMS Collaboration], Phys. Lett. B **718**, 348 (2012) [arXiv:1210.1797 [hep-ex]].
- [24] [ATLAS Collaboration], ATLAS-CONF-2013-019.
- [25] R. N. Mohapatra, Phys. Rev. Lett. **56**, 561 (1986); R. N. Mohapatra and J. W. F. Valle, Phys. Rev. D **34**, 1642 (1986).
- [26] M. Malinsky, J. C. Romao and J. W. F. Valle, Phys. Rev. Lett. **95**, 161801 (2005) [hep-ph/0506296].
- [27] P. S. B. Dev and A. Pilaftsis, Phys. Rev. D **86**, 113001 (2012) [arXiv:1209.4051 [hep-ph]].
- [28] For early literature on detection at a hadron collider of right-handed neutrinos in the left-right symmetric theory, see: W. -Y. Keung and G. Senjanovic, Phys. Rev. Lett. **50**, 1427 (1983).
- [29] A. Arhrib, B. Bajc, D. K. Ghosh, T. Han, G. -Y. Huang, I. Puljak and G. Senjanovic, Phys. Rev. D **82**, 053004 (2010) [arXiv:0904.2390 [hep-ph]].
- [30] B. Bajc, M. Nemevsek and G. Senjanovic, Phys. Rev. D **76**, 055011 (2007) [hep-ph/0703080].
- [31] T. Han, I. Lewis, R. Ruiz and Z. -g. Si, Phys. Rev. D **87**, 035011 (2013) [Erratum-ibid. D **87**, no. 3, 039906 (2013)] [arXiv:1211.6447 [hep-ph]].
- [32] S. Bar-Shalom, G. Eilam, T. Han and A. Soni, Phys. Rev. D **77**, 115019 (2008) [arXiv:0803.2835 [hep-ph]].
- [33] P. Fileviez Perez, T. Han and T. Li, Phys. Rev. D **80**, 073015 (2009) [arXiv:0907.4186 [hep-ph]].

- [34] F. del Aguila and M. Chala, arXiv:1311.1510 [hep-ph].
- [35] P. S. B. Dev, C. -H. Lee and R. N. Mohapatra, Phys. Rev. D **88**, 093010 (2013) [arXiv:1309.0774 [hep-ph]].
- [36] A. Zee, Phys. Lett. B **93**, 389 (1980) [Erratum-ibid. B **95**, 461 (1980)];
A. Zee, Nucl. Phys. B **264**, 99 (1986); K. S. Babu, Phys. Lett. B **203**, 132 (1988).
- [37] L. M. Krauss, S. Nasri and M. Trodden, Phys. Rev. D **67**, 085002 (2003) [arXiv:hep-ph/0210389];
K. Cheung and O. Seto, Phys. Rev. D **69**, 113009 (2004) [arXiv:hep-ph/0403003]; M. Aoki, S. Kanemura and O. Seto, Phys. Rev. Lett. **102**, 051805 (2009) [arXiv:0807.0361 [hep-ph]]; Phys. Rev. D **80**, 033007 (2009) [arXiv:0904.3829 [hep-ph]].
- [38] E. Ma, Phys. Rev. D **73**, 077301 (2006) [arXiv:hep-ph/0601225].
- [39] P. Fileviez Perez and M. B. Wise, Phys. Rev. D **80**, 053006 (2009) [arXiv:0906.2950 [hep-ph]].
- [40] P. Fileviez Perez, T. Han, S. Spinner and M. K. Trenkel, JHEP **1101**, 046 (2011) [arXiv:1010.5802 [hep-ph]].
- [41] Y. Liao, Phys. Lett. B **694**, 346 (2011) [arXiv:1009.1692 [hep-ph]].
- [42] K. S. Babu and C. N. Leung, Nucl. Phys. B **619**, 667 (2001) [arXiv:hep-ph/0106054]; E. Ma, Phys. Rev. D **66**, 037301 (2002) [arXiv:hep-ph/0204013]; I. Gogoladze, N. Okada and Q. Shafi, Phys. Lett. B **672**, 235 (2009) [arXiv:0809.0703 [hep-ph]]; A. de Gouvea and J. Jenkins, Phys. Rev. D **77**, 013008 (2008) [arXiv:0708.1344 [hep-ph]]; W. Grimus, L. Lavoura and B. Radovcic, Phys. Lett. B **674**, 117 (2009) [arXiv:0902.2325 [hep-ph]]; P. H. Gu, H. J. He, U. Sarkar and X. m. Zhang, Phys. Rev. D **80**, 053004 (2009) [arXiv:0906.0442 [hep-ph]]; Z. z. Xing and S. Zhou, Phys. Lett. B **679**, 249 (2009) [arXiv:0906.1757 [hep-ph]]; F. Bonnet, D. Hernandez, T. Ota and W. Winter, JHEP **0910**, 076 (2009) [arXiv:0907.3143 [hep-ph]]; I. Picek and B. Radovcic, Phys. Lett. B **687**, 338 (2010) [arXiv:0911.1374 [hep-ph]]; K. L. McDonald, JHEP **1307**, 020 (2013) [arXiv:1303.4573 [hep-ph]]; S. S. C. Law and K. L. McDonald, Phys. Rev. D **87**, 113003 (2013) [arXiv:1303.4887 [hep-ph]].
- [43] K. S. Babu, S. Nandi and Z. Tavartkiladze, Phys. Rev. D **80**, 071702 (2009) [arXiv:0905.2710 [hep-ph]].
- [44] Y. Liao, JHEP **1106**, 098 (2011) [arXiv:1011.3633 [hep-ph]].
- [45] Y. Liao and J. -Y. Liu, Phys. Rev. D **81**, 013004 (2010) [arXiv:0911.3711 [hep-ph]].
- [46] R. Kitano, M. Koike and Y. Okada, Phys. Rev. D **66**, 096002 (2002) [Erratum-ibid. D **76**, 059902 (2007)] [hep-ph/0203110].
- [47] J. Adam *et al.* [MEG Collaboration], arXiv:1303.0754 [hep-ex].

- [48] U. Bellgardt *et al.* [SINDRUM Collaboration], Nucl. Phys. B **299**, 1 (1988).
- [49] J. Beringer *et al.* [Particle Data Group Collaboration], Phys. Rev. D **86**, 010001 (2012).
- [50] L. Willmann, P. V. Schmidt, H. P. Wirtz, R. Abela, V. Baranov, J. Bagaturia, W. H. Bertl and R. Engfer *et al.*, Phys. Rev. Lett. **82**, 49 (1999) [hep-ex/9807011].
- [51] T. Fukuyama, H. Sugiyama and K. Tsumura, JHEP **1003**, 044 (2010) [arXiv:0909.4943 [hep-ph]].
- [52] N. D. Christensen and C. Duhr, Comput. Phys. Commun. **180**, 1614 (2009) [arXiv:0806.4194 [hep-ph]].
- [53] J. Alwall, M. Herquet, F. Maltoni, O. Mattelaer and T. Stelzer, JHEP **1106**, 128 (2011) [arXiv:1106.0522 [hep-ph]].
- [54] T. Sjostrand, S. Mrenna and P. Z. Skands, JHEP **0605**, 026 (2006) [hep-ph/0603175].
- [55] E. Conte, B. Fuks and G. Serret, Comput. Phys. Commun. **184**, 222 (2013) [arXiv:1206.1599 [hep-ph]].
- [56] P. M. Nadolsky, H. -L. Lai, Q. -H. Cao, J. Huston, J. Pumplin, D. Stump, W. -K. Tung and C. -P. Yuan, Phys. Rev. D **78** (2008) 013004 [arXiv:0802.0007 [hep-ph]].
- [57] M. Muhlleitner and M. Spira, Phys. Rev. D **68**, 117701 (2003) [hep-ph/0305288].
- [58] S. Hoeche, F. Krauss, N. Lavesson, L. Lonnblad, M. Mangano, A. Schaliche and S. Schumann, hep-ph/0602031.
- [59] C. -S. Chen and Y. -J. Zheng, arXiv:1312.7207 [hep-ph].